



Eastern margin of the Ross Sea Rift in western Marie Byrd Land, Antarctica: Crustal structure and tectonic development

Bruce P. Luyendyk

Department of Geological Sciences and Institute for Crustal Studies, University of California, Santa Barbara, California 93106, USA (luyendyk@geology.ucsb.edu)

Douglas S. Wilson

Department of Geological Sciences, Marine Science Institute, Institute for Crustal Studies, University of California, Santa Barbara, California 93106, USA

Also at Marine Science Institute, University of California, Santa Barbara, California 93106, USA

Christine S. Siddoway

Department of Geology, Colorado College, Colorado Springs, Colorado 80903, USA

[1] The basement rock and structures of the Ross Sea rift are exposed in coastal western Marie Byrd Land (wMBL), West Antarctica. Thinned, extended continental crust forms wMBL and the eastern Ross Sea continental shelf, where faults control the regional basin-and range-type topography at ~ 20 km spacing. Onshore in the Ford Ranges and Rockefeller Mountains of wMBL, basement rocks consist of Early Paleozoic metagreywacke and migmatized equivalents, intruded by Devonian-Carboniferous and Cretaceous granitoids. Marine geophysical profiles suggest that these geological formations continue offshore to the west beneath the eastern Ross Sea, and are covered by glacial and glacial marine sediments. Airborne gravity and radar soundings over wMBL indicate a thicker crust and smoother basement inland to the north and east of the northern Ford Ranges. A migmatite complex near this transition, exhumed from mid crustal depths between 100–94 Ma, suggests a profound crustal discontinuity near the inboard limit of extended crust, ~ 300 km northeast of the eastern Ross Sea margin. Near this limit, aeromagnetic mapping reveals an extensive region of high amplitude anomalies east of the Ford ranges that can be interpreted as a sub ice volcanic province. Modeling of gravity data suggests that extended crust in the eastern Ross Sea and wMBL is 8–9 km thinner than interior MBL ($\beta = 1.35$). Gravity modeling also outlines extensive regions of low-density ($2300\text{--}2500 \text{ kg m}^{-3}$) buried basement rock that is lighter than rock exposed at the surface. These regions are interpreted as bounded by throughgoing east-west faults with vertical separation. These buried low-density rocks are possibly a low-density facies of Early Paleozoic metagreywacke, or the low-density epizonal facies of Cretaceous granites, or felsic volcanic rocks known from moraines. These geophysical features and structures on land in the wMBL region preserve the record of middle and Late Cretaceous development of the Ross Sea rift. Thermochronology data from basement rocks and offshore stratigraphy suggest that the wMBL rift margin formed and most extension occurred in mid- and Late Cretaceous time, before seafloor spreading initiated between wMBL and the Campbell Plateau. The Cretaceous tectonic record in wMBL contrasts with the Transantarctic Mountains that form the western rift margin, where significant rift-flank relief developed in middle Tertiary time.

Components: 11,444 words, 8 figures.

Keywords: Ross Sea; Marie Byrd Land; Antarctica.

Index Terms: 9310 Information Related to Geographic Region: Antarctica; 8109 Tectonophysics: Continental tectonics—extensional (0905); 8105 Tectonophysics: Continental margins and sedimentary basins (1212).

Received 17 October 2002; **Revised** 24 April 2003; **Accepted** 15 August 2003; **Published** 29 October 2003.

Luyendyk, B. P., D. S. Wilson, and C. S. Siddoway, Eastern margin of the Ross Sea Rift in western Marie Byrd Land, Antarctica: Crustal structure and tectonic development, *Geochem. Geophys. Geosyst.*, 4(10), 1090, doi:10.1029/2002GC000462, 2003.

1. Introduction

1.1. The Ross Sea Rift

[2] The Ross Sea Embayment, occupied by the Ross Ice Shelf and the Ross Sea (Figure 1a), defines part of the boundary zone between East and West Antarctica. Its subsided crust constitutes a major portion of the West Antarctic Rift system [LeMasurier and Rex, 1990; Tessensohn and Worner, 1991; Storey *et al.*, 1999] an area of extended lithosphere between the East Antarctic craton and the microplates of Pacific West Antarctica [Dalziel and Elliot, 1982]. Major tectonic activity in the Ross Sea rift occurred in middle (late Early to early Late) Cretaceous time [Davey and Brancolini, 1995; Fitzgerald and Baldwin, 1997; Luyendyk *et al.*, 2001] brought about by the rifting of Gondwana. Activity in Cenozoic time was focused in the western side of the rift [Cande *et al.*, 2000; Hamilton *et al.*, 2001].

[3] The Ross Sea rift is bounded on the east by western Marie Byrd Land (wMBL) and on the west by the Transantarctic Mountains. Whereas bedrock elevations in wMBL are rarely more than 1000 m, the Transantarctic Mountains rise abruptly to heights of 4000 m above the western Ross Sea. This contrast is dramatic and indicates that the Ross Sea rift is asymmetric in structure and tectonic history. However, the actual architecture and tectonic history of the eastern rift, and the question whether the asymmetry developed in a single or multiple events have been largely unknown until recently. Deciphering the history and structural framework for the eastern rift has been our goal in a series of studies in wMBL over the past decade. These studies have included geological mapping [Luyendyk *et al.*, 1992], thermochronology

[Richard *et al.*, 1994], paleomagnetism [Luyendyk *et al.*, 1996], surface gravity [Luyendyk *et al.*, 2003], structural geology [Siddoway, 1999; Whitehead *et al.*, 1999], offshore marine geophysics [Luyendyk *et al.*, 2001], and most recently our airborne geophysics [Wilson *et al.*, 2000] that is covered in detail here. Knowledge of wMBL evolution bears on plate tectonic reconstructions for the southern Pacific Ocean and New Zealand [Stock and Cande, 2002], Antarctic paleogeography, and boundary conditions for the West Antarctic ice sheet [Dalziel and Lawver, 2001].

1.2. Geology of Coastal Western Marie Byrd Land

[4] Outcrops in coastal wMBL occur in the Rockefeller Mountains and scattered nunataks on Edward VII Peninsula and in the Ford Ranges (Figures 1a, 1b, and 2a). Individual ranges reach elevations of 1000 m or more, are aligned E-W or NW-SE, and are separated by glaciers 500 m to over 1000 m thick. Rocks here comprise Early Paleozoic low-grade greywacke and argillite of the Swanson Formation, Devonian Ford Granodiorite, Cretaceous Byrd Coast Granite, Cretaceous mafic dikes, and minor Neogene (Pleistocene) volcanic rocks, primarily basalt [Bradshaw *et al.*, 1983; Adams *et al.*, 1995; Pankhurst *et al.*, 1998; Weaver *et al.*, 1991, 1994; Luyendyk *et al.*, 1992; Wade *et al.*, 1977a, 1977b, 1977c, 1978]. Locally the Byrd Coast Granite exhibits distinctive textures suggestive of epizonal emplacement; namely, a porphyritic phase with an aphanitic groundmass (hypabyssal volcanic texture), smoky quartz crystals with terminations and miarolitic pockets. The mafic dikes throughout the Ford Ranges (Fosdick Mountains excluded) have a regional trend of N12W [Siddoway *et al.*, 2003]. The Flood and

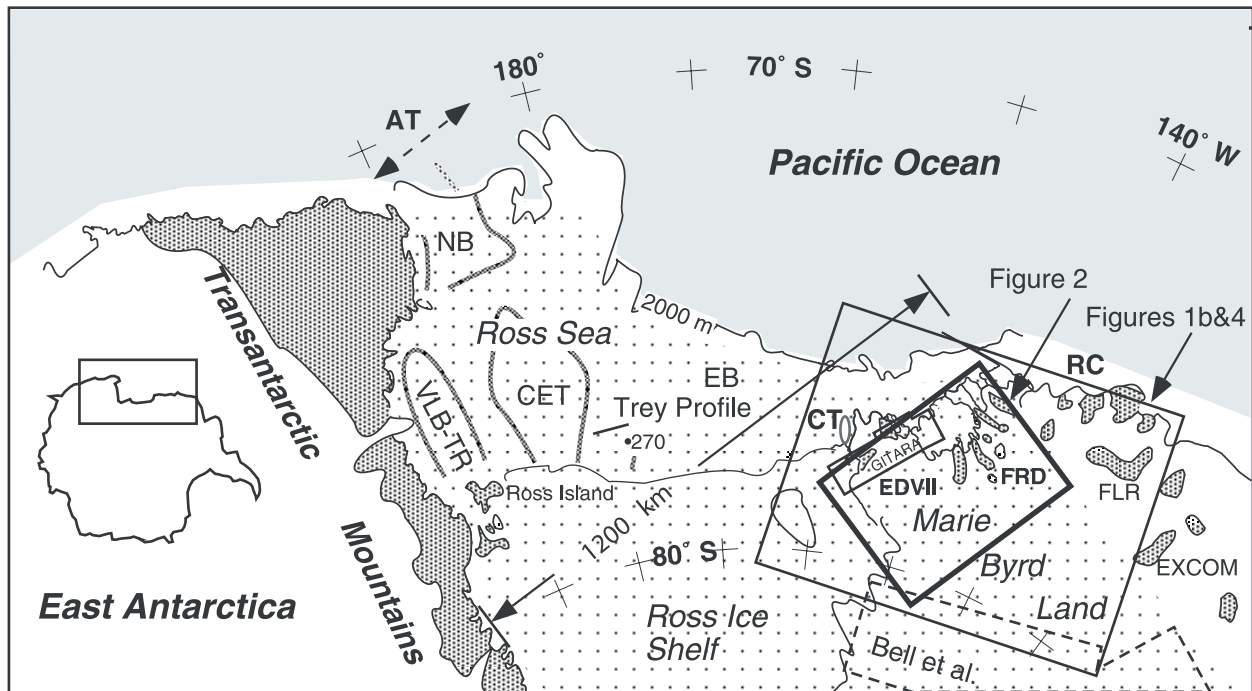


Figure 1. (a) Ross Sea region map (polar stereographic projection) showing Marie Byrd Land and the Ross Embayment (=Ross Sea plus Ross Ice Shelf), the location of our study area (Figures 1b, 2 and 4), and airborne geophysical survey (heavy box), the airborne survey of *Bell et al.* (dashed box) [*Bell et al.*, 1999], the aeromagnetic survey of *Ferraccioli et al.* [2002] (GITARA), geophysical profile of *Trey et al.* [1999], outcrop onshore (dark shaded), Deep Sea Drilling Site 270, and the Transantarctic Mountains. AT, Adare Trough (dashed arrows indicate former spreading directions; [*Cande et al.*, 2000]). Major basins are outlined; VLB-TR, Victoria Land Basin including the Terror Rift; NB, Northern Basin; CET, Central Trough; EB, Eastern Basin; EDVII, Edward VII Peninsula; CT, Colbeck Trough; FRD, Ford Ranges; FLR, Flood Ranges; EXCOM, Executive Committee Range; RC, Ruppert Coast. The West Antarctic and Ross Sea Rift system is outlined by the light shade [*LeMasurier and Rex*, 1990] increased in width here to include the Ford Ranges. We interpret the rift to be 1200 km wide across the Ross Embayment. (b) Elevations above sea level from our airborne radar soundings and DEM of *Liu et al.* [1999]. Box outlines location of our airborne geophysics survey. Dashed box is GITARA aeromagnetic survey of *Ferraccioli et al.* [2002]. Red outlines are grounding line (heavy) and ice shelf edge (orange light). Outcrops and ranges are shown in black. Lambert conic projection. Contour interval 250 meters.

Executive Committee Ranges farther east (Figure 1a) are Neogene and Quaternary volcanic centers [*LeMasurier and Rex*, 1989; *LeMasurier and Rex*, 1990; *Panter et al.*, 2000]. Silicic pyroclastic volcanic rocks (rhyolite) are known from glacial drift in the Fosdick Mountains [*Cowdery and Stone*, 2001] and from erratics recovered by dredge offshore but they do not crop out. One erratic has a $^{40}\text{Ar}/^{39}\text{Ar}$ sanidine age of 930 ± 36 ka (R. P. Esser, unpublished data report, New Mexico Geochronology Research Lab, 2001).

[5] Migmatites form the Fosdick Mountains (Figure 2a) of the northern Ford Ranges, where cordierite-sillimanite-garnet assemblages record metamorphic temperatures of $\sim 700^\circ\text{C}$ and depths

of 16–20 km in the middle crust [*Smith*, 1992, 1997]. Peak metamorphism at 105 Ma [*Richard et al.*, 1994] was followed soon after by faulting, tilting [*Richard et al.*, 1994; *Luyendyk et al.*, 1996], and exhumation of the mid-crustal rocks between 100 and 94 Ma, based on middle Cretaceous $^{40}\text{Ar}/^{39}\text{Ar}$ cooling ages [*Richard et al.*, 1994]. *Richard et al.* [1994] in summarizing their findings from structural geology and thermochronology conclude that the migmatites originated in an extensional environment but the range lacks the structures characteristic of a Cordilleran-type core complex like those in the western North America. Sub-vertical mafic dikes in the Fosdick Mountains oriented N78E (mean; C. Siddoway observations) record NNE stretching across the migmatite dome.

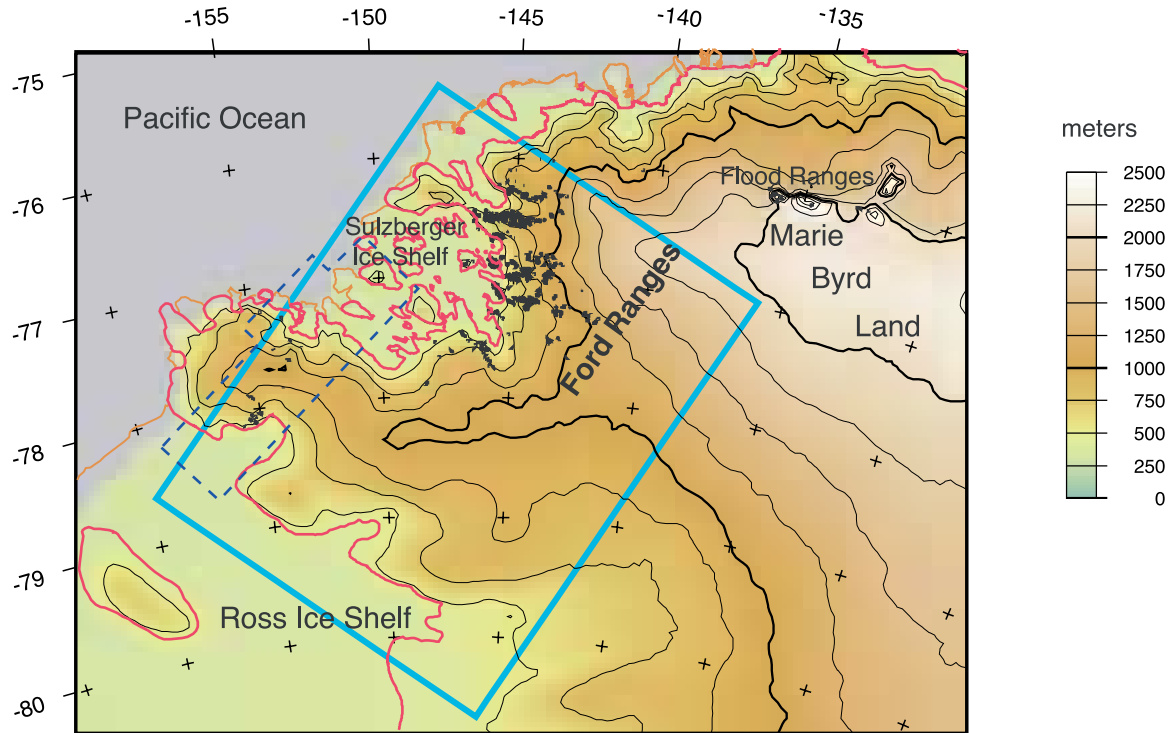


Figure 1. (continued)

[6] The Phillips Mountains, located immediately north of the Fosdick Mountains (Figure 2a), consist in part of Ford Granodiorite and Byrd Coast Granite that show no evidence of dynamic metamorphism. Cooling data suggest these mountains were at a shallower crustal level than the Fosdick range in Cretaceous time [Richard *et al.*, 1994]. This suggests a crustal boundary between these two ranges and that the Phillips Mountains form the hanging wall of a major fault zone [Luyendyk *et al.*, 1992; Richard *et al.*, 1994].

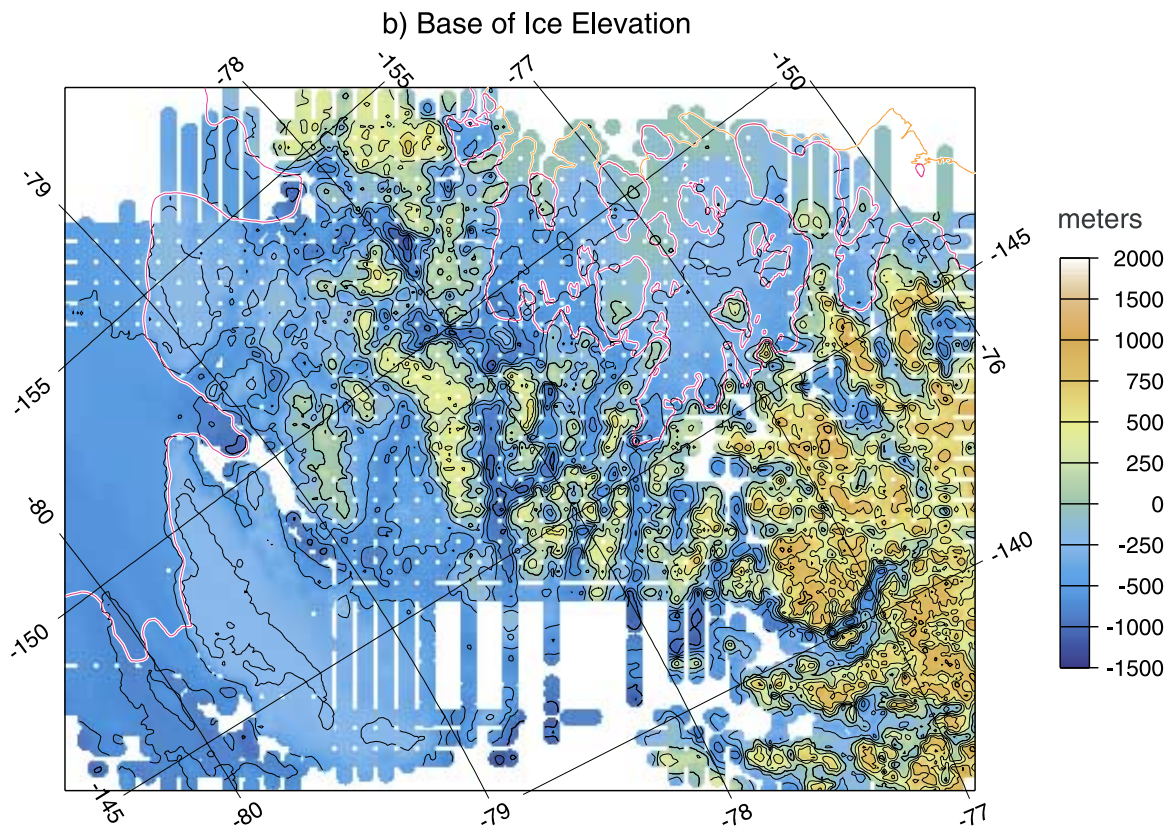
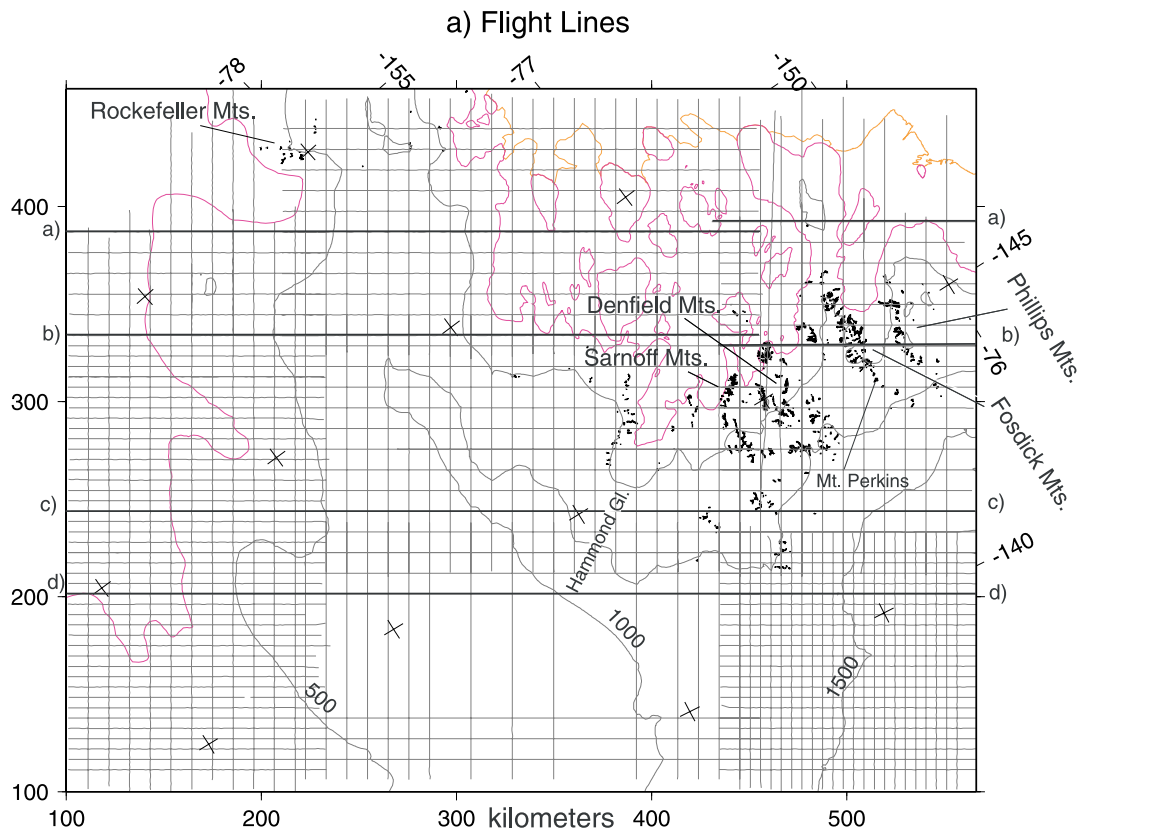
[7] Sparse gravity data imply that the region of the Ford Ranges is underlain by thin crust [Bentley, 1973; Bentley, 1991; Behrendt *et al.*, 1991a]. Prior gravity studies show the densest crust to underlie the Fosdick Mountain range [Beitzel, 1972; Luyendyk *et*

al., 2003], potentially a sign of mafic magmatism in the lower crust [e.g., Smith, 1997].

2. Airborne Surveys

[8] During December 1998 through February 1999, the SOAR project (Support Office for Aero-geophysical Research at the University of Texas, Austin) flew an airborne geophysics survey of western Marie Byrd Land (Figures 1a, 1b, and 2a) collecting radar echo soundings to measure surface elevation (Figure 1b) and ice thickness (Figure 2b), along with magnetics (Figure 2c) and gravity (Figure 2d), over an area extending 470 km (NE-SW) by 350 km (NW-SE). The survey included most of Edward VII Peninsula and all of the Ford Ranges. Track spacing over most of the area was 5.3 or 10.6 km (Figure 2a). Bell *et al.*

Figure 2. (opposite) (a) Aero-geophysical track lines showing kilometer grid coordinates used with origin in the extreme south corner. Surface elevation in meters above sea level, contour interval 500 meters. Grounding line shown in magenta and ice edges in orange. Gravity profiles shown in Figures 5a–5d are indicated. (b) Elevation of base of ice above sea level from airborne radar sounding (see text). Outside of the grounding line (magenta) floating ice shows a smooth base. (c) Magnetic anomaly in nanotesla. See text for survey details. Box at grid top marks overlap with GITARA survey [Ferraccioli *et al.*, 2002]. (d) Free Air gravity anomaly in milligals; see text for survey details.



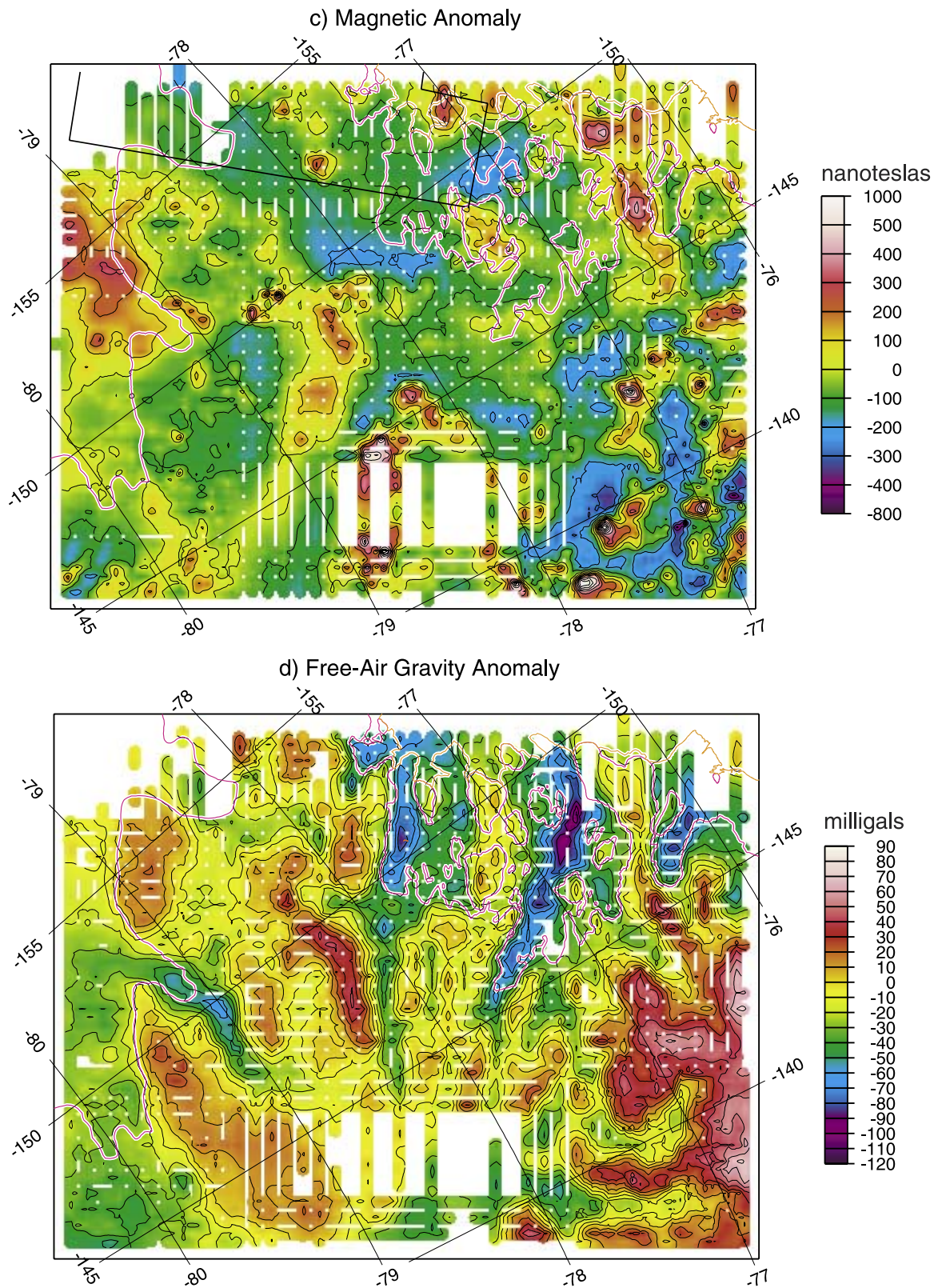


Figure 2. (continued)

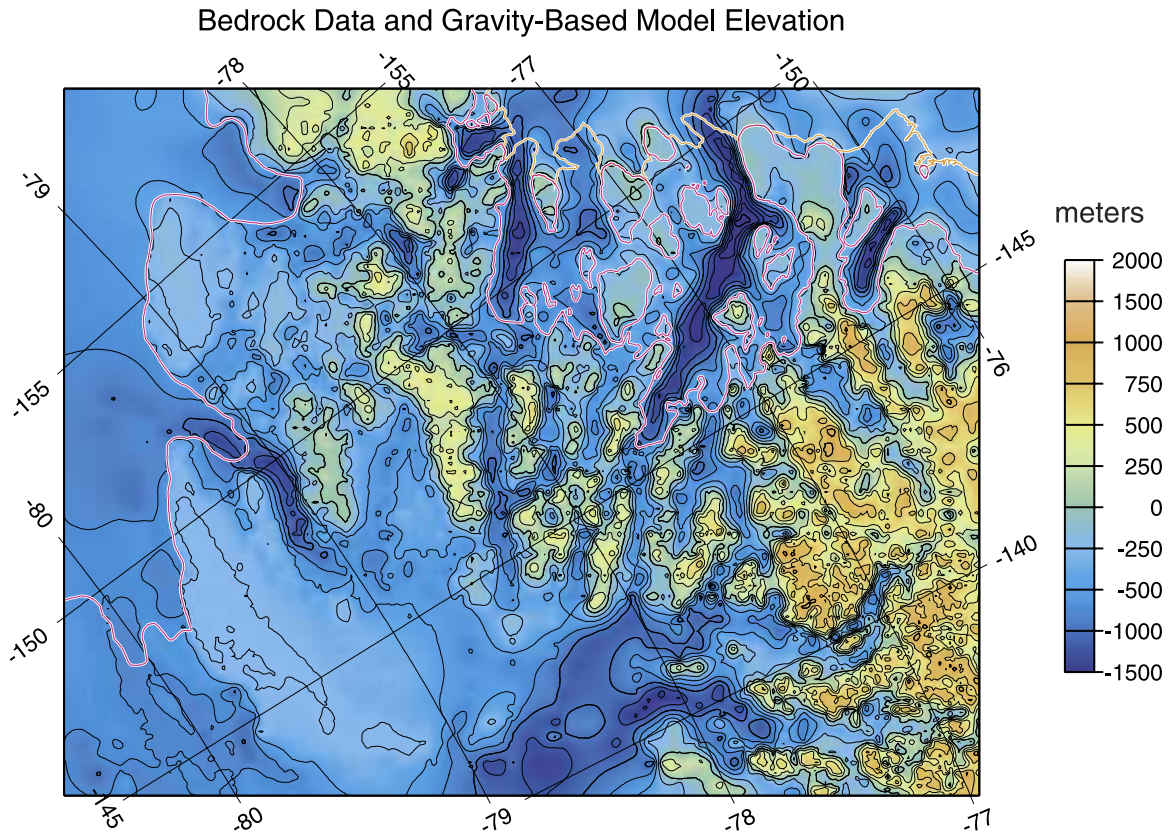


Figure 3. Bedrock elevations and bathymetry relative to sea level in western Marie Byrd Land survey area (Figures 1 and 2). Elevation from airborne radar soundings and modeling of gravity over floating ice and over radar reflection gaps; contour interval 250 meters.

[1999] have described instrumentation of the aircraft and data reduction procedures. Flight elevation varied to maintain a minimum of 300 m above local topography, and speed was about 130 knots (67 m/s).

2.1. Airborne Radar

[9] Radar echo soundings were averaged to an interval of 4–5 pings per second prior to digitizing topography and ice thickness. Ice thickness is derived using a radar velocity of 168.4 m/ μ s, with an estimated correction of 10 m added for faster velocity in firn. Quantitative analysis of the airborne survey data is based on gridding the observations at 1.06-km node spacing (1/5 or 1/10 of standard track spacing) with 441 \times 341 nodes total grid size.

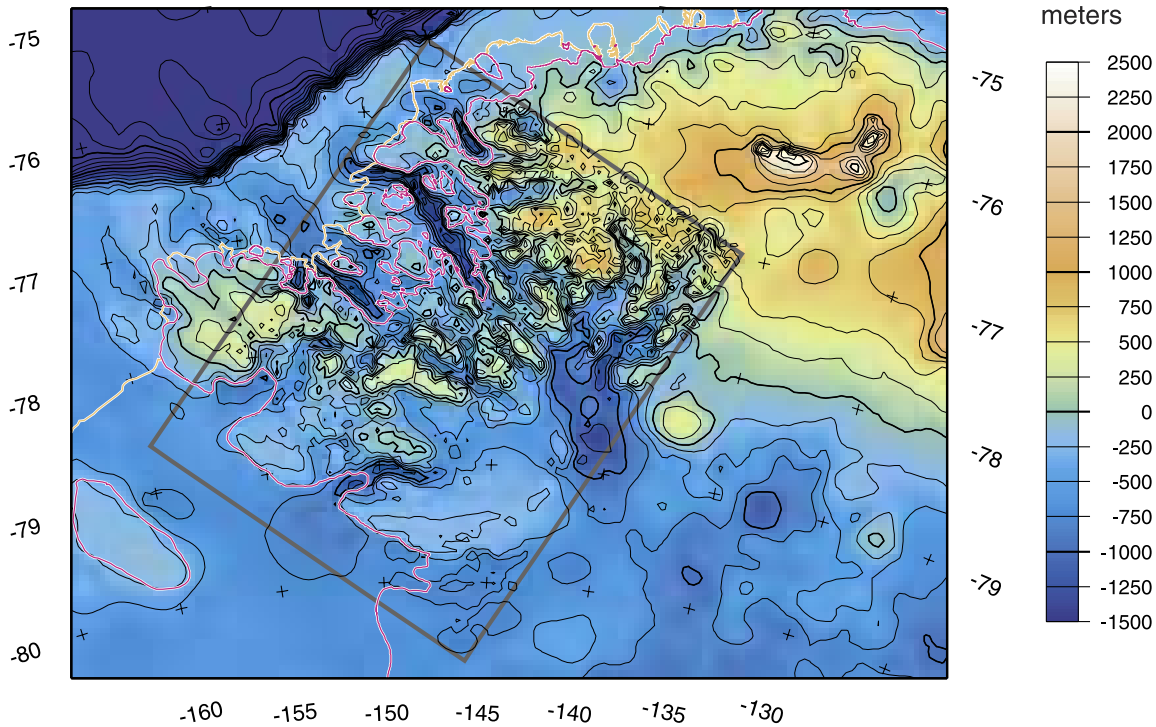
[10] The ice surface rises gradually from just above sea level to almost 2000 meters elevation at the

northeast side of the survey area (Figure 1b). The bedrock surface we mapped from radar data also rises toward the interior of wMBL from below sea level under most of Edward VII Peninsula to 700–1000 m (Figure 2b). Under the Ford Ranges the bedrock topography is arranged in NW-SE and E-W trending ranges and linear valleys occupied by outlet glaciers. Relief is 1 km or more at a spacing of 20 to 30 km (Figure 2b). A level bedrock plateau at about 250 m meters below sea level marks the boundary between wMBL and the Ross Embayment (Figure 2b). This is interpreted as a Late Tertiary wave-cut surface [Wilson *et al.*, 2003]. Basement relief under the ice shelves where radar returns were absent was modeled using the gravity data (Figure 3; discussed below).

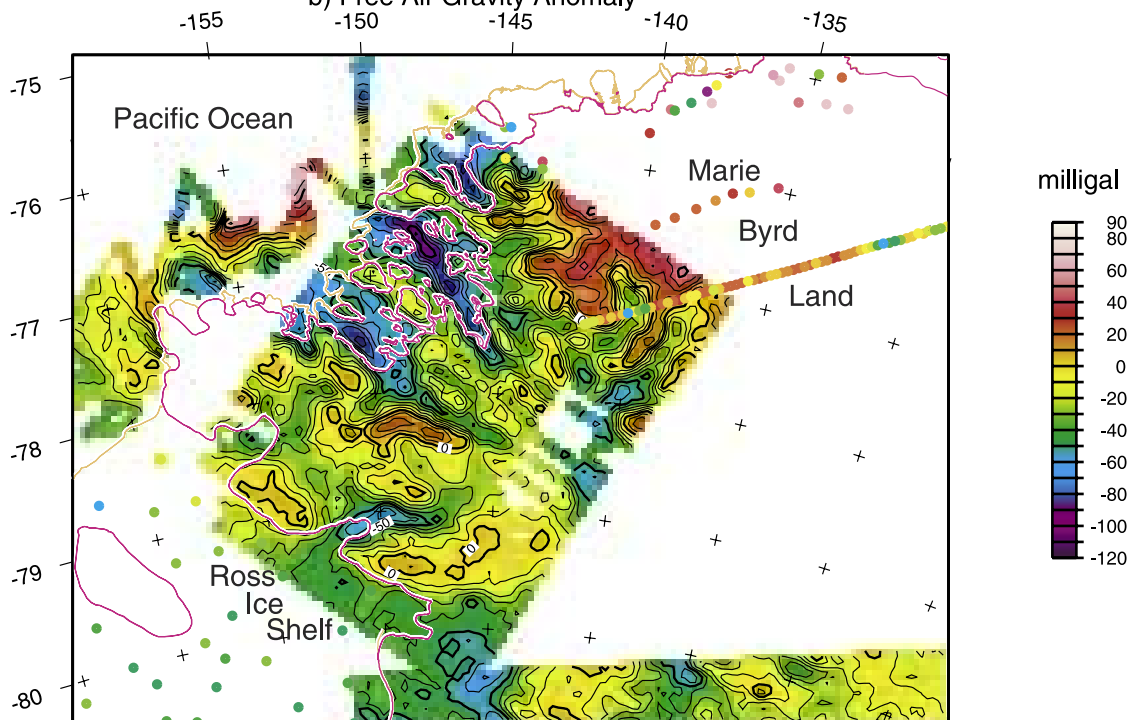
2.2. Aeromagnetic Data

[11] Aeromagnetic data were collected simultaneously with the other measurements (Figure 2c).

a) Bedrock Elevation and Bathymetry



b) Free Air Gravity Anomaly



The data will be the subject of more in-depth analysis in a subsequent paper. Instrumentation was a Cesium-vapor magnetometer with a sample rate of 1 second. Magnetic data were corrected for diurnal variation measured at the aircraft base camp and reduced to IGRF 1995. After crossover correction, typical crossover error is about 15 nT.

[12] Our magnetic survey overlaps the northeastern portion of the aeromagnetic survey completed on the northern Edward VI Peninsula by *Ferraccioli et al.* [2002]. Mapping reveals two classes of anomalies (Figures 2c and 6 below). One class is those anomalies of less than 500 nT amplitude and wavelengths of 25 km or more (low amplitude – low gradient). They are elongate in map view. These are similar to anomalies mapped by *Ferraccioli et al.* [2002] and are found in the western half of the survey area. The other class is shorter-wavelength anomalies of generally higher amplitude (up to 900 nT) that are approximately circular with diameters less than 20 km (high amplitude - high gradient). These are generally located in the eastern half of the survey in ice-covered regions (Figure 2c). The second class is clearly caused primarily by highly magnetic volcanic centers beneath the ice. Modeling by *Ferraccioli et al.* [2002] demonstrated the likely cause of the first type is basement magnetization contrast between plutonic rocks. The high amplitude anomalies are not likely due to plutonic rocks because the magnetization strength of all types of these rocks we collected is far too weak to explain them ($K < 0.001$ (SI); $M < 0.01$ A/m).

We did measure magnetic properties of volcanic rocks of Mount Perkins, a Pleistocene composite cone in the eastern Fosdick Mountains (Figure 2a). The magnetization strength of those rocks is high ($K \cong 0.01$; $M \cong 1.0$ A/m) and consistent with other common volcanic rocks. Therefore we infer that the dozen or so high amplitude anomalies in the eastern and northeastern part of the survey, east of Mount Perkins (Figure 2a), locate a previously unmapped volcanic province of unknown but possibly young age now covered by the ice sheet.

2.3. Airborne Gravity Data

[13] Gravity readings need large corrections for acceleration of the aircraft, and the data required filtering to remove short-wavelength imperfections in the corrections. The frequency domain filter we used [*Childers et al.*, 1999] passes angular frequencies below 0.003 s^{-1} and cuts angular frequencies above 0.006 s^{-1} , cutting spatial wavelengths below about 10 km and passing above about 20 km. After filtering, subjective editing is required to remove remaining spikes that are often correlated with the less-straight parts of the flight lines. After crossover correction, typical (1-sigma) crossover error is about 5 mgal. The gravity base level was determined by crossover comparison with five Ross Ice Shelf stations from *Greischar et al.* [1992], Sulzberger Ice Shelf stations from *Luyendyk et al.* [2003], and one unpublished marine profile (NBP 94-02), in all cases at sites where the gravity gradient is low enough that filter effects for the airborne data are minor.

Figure 4. (opposite) (a) Bedrock elevations and bathymetry in western Marie Byrd Land. Elevation inside survey area from airborne radar soundings and modeling of gravity over floating ice and over radar reflection gaps (Figure 3); outside survey area from BEDMAP compilation [*Lythe et al.*, 2001] (<http://www.antarctica.ac.uk/bedmap/>) and new compilation of marine soundings in the Ross Sea [*Luyendyk et al.*, 2002] along with *Palmer* cruise 03-01. Contour interval 250 meters. (b) Free Air anomaly from our airborne survey and others to the south [*Bell et al.*, 1999], [*Studinger et al.*, 2002], supplemented by onshore gravity observations from surface traverses [*Beitzel*, 1972; *Behrendt et al.*, 1991b; *Luyendyk et al.*, 2003]. Stations on Ross Ice Shelf are from *Greischar et al.* [1992]. Offshore gravity observations are from our marine survey [*Luyendyk et al.*, 2001] and others. (c) Bouguer gravity anomaly based on densities of ice = 900 kg m^{-3} , water = 1030 kg m^{-3} and bedrock = 2670 kg m^{-3} . Anomaly was not plotted where bedrock elevations were not directly observed. Bouguer gravity is lowest where elevation is highest. (d) Depth to Moho model computed iteratively from multilayer model of ice, water, sediments = 2300 kg m^{-3} , upper basement = 2670 kg m^{-3} , lower basement of 2950 kg m^{-3} , and mantle = 3330 kg m^{-3} . Locations of profiles in Figure 5 are shown. Moho depth is calibrated to Ross Sea measurement of *Trey et al.* (Figure 1) [*Trey et al.*, 1999]. Offshore Moho model modified from *Luyendyk et al.* [2001]. Contour interval 1 km. Deeper Moho contours to east are assumed to follow basement contours (Figure 4a). This region represents thicker and less extended crust.

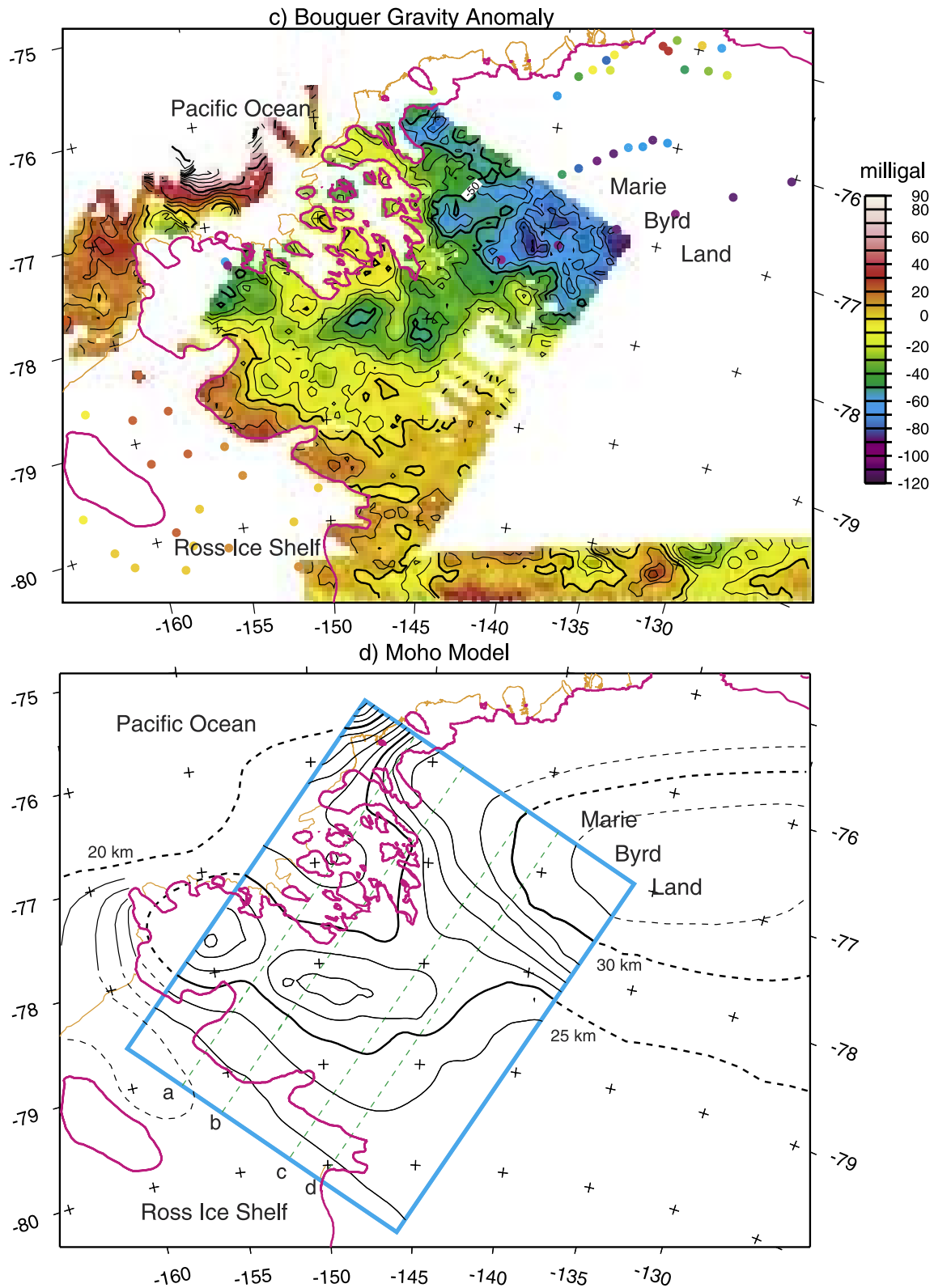


Figure 4. (continued)

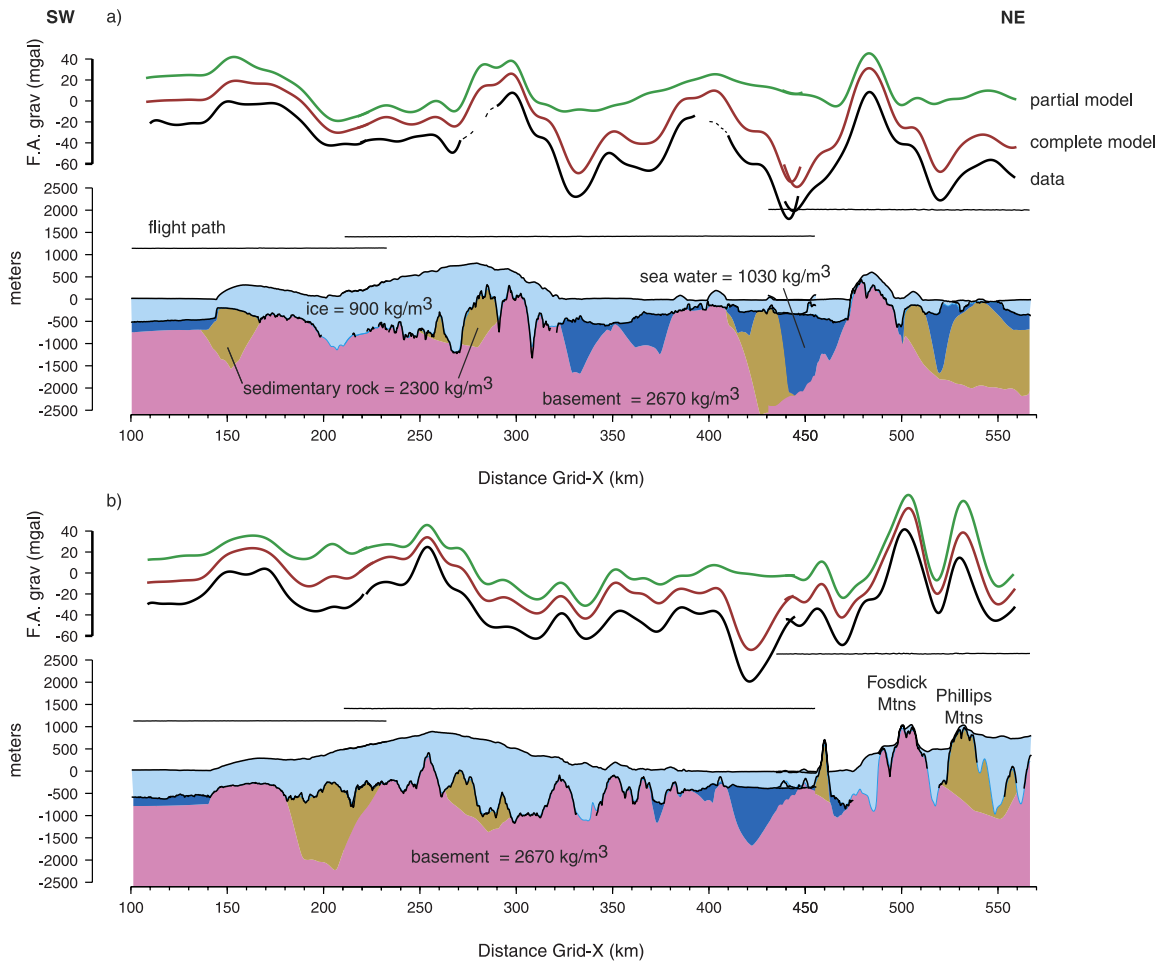


Figure 5. Free air anomaly data profiles (black lines) are compared with gravity predictions based on models with ice, basement, and mantle layers (green lines), and with ice, water, sediment, basement and mantle layers (red lines). The predicted profiles have been offset upward for more convenient viewing. Cross sections show radar reflection data as black lines and layer types by color. Both the observed and predicted anomalies have been filtered to remove wavelengths less than about 10 km. In several areas, adding water and sediment layers dramatically improves the agreement between model and data. Profile locations are shown in Figure 2a. Two observed profiles (offset of 5.3 km; Figure 2a) have been joined at their NE ends to form a single profile.

Elevations of surface and bed topography and of the aircraft for the free-air gravity correction have been adjusted from the original WGS84 reference frame to sea level using the EGM96 geoid [Lemoine *et al.*, 1998].

[14] Free Air gravity rises to above 50 mgals and Bouguer gravity falls to below -100 mgals eastward from the Ford Ranges toward interior wMBL (Figure 4). Iterative forward modeling was performed using the gravity data to determine crustal structure and Moho depth. We were able to derive good estimates of several parameters that

strongly influence the gravity field, including bed topography under floating ice (Figures 3 and 4a), Moho topography (Figure 4d), and the distribution of low-density bedrock and crust (Figures 5 and 6). Gravity models were calculated in the frequency domain using the technique of Parker [Parker, 1973] for interfaces such as air/ice and ice/basement, on grids padded to 512×384 nodes. Complete models are calculated adding the effects of multiple interfaces, namely air/ice, ice/water, water/bedrock, and Moho, with several interfaces constrained to coincide where layers are missing, for example at basement outcrops. Several inter-

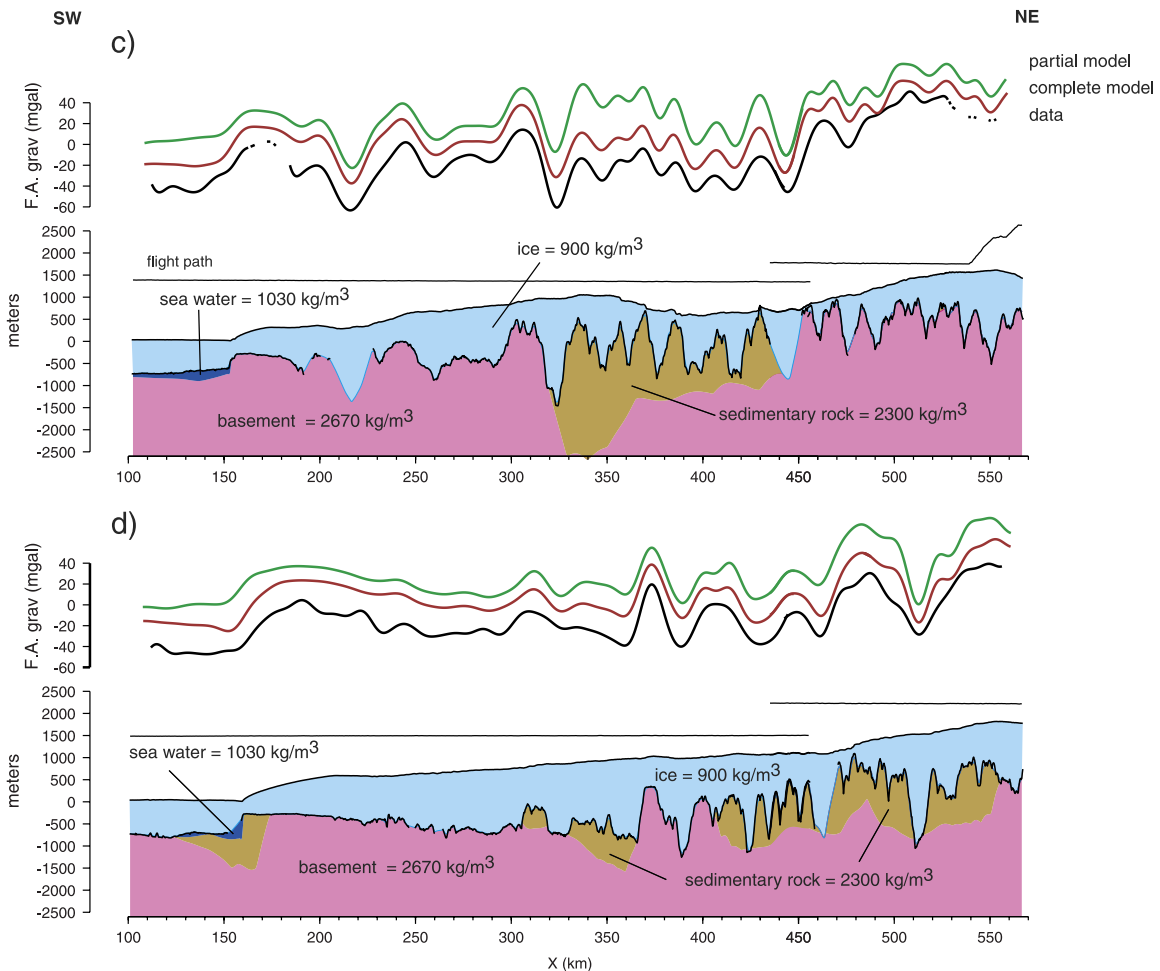


Figure 5. (continued)

faces include subjective input either to fill data gaps, such as the ice/bedrock interface in areas of thick ice and weak bedrock radar echoes, or due to total absence of data, such as for the Moho interface. These subjective inputs were then adjusted iteratively to produce a new interface grid that predicts gravity anomalies closer to those observed. Because the gravity data have been significantly filtered to reduce the effects of short-period aircraft accelerations, we also filtered model values in the same manner in order to compare models with data profiles (Figure 5).

[15] The simplest and most confident inference from this type of gravity survey involves mapping steep changes in water depth under floating ice. The Sulzberger Ice Shelf (Figure 1a), which to our

knowledge has no seismic soundings of the water thickness below the ice, shows fairly linear and strongly negative free air anomalies near its southwestern and northeastern margins (Figure 2d). Gravity models (Figures 5a–5b) are consistent with these anomalies being caused by glacially carved troughs reaching depths generally greater than 1400 m and up to about 2200 m [Wilson *et al.*, 2001]. These model profiles are 2-D samples of the 3-D forward model, with the predicted gravity filtered identically to the gravity data. For simplicity, we assume that these troughs are not partially filled with young, glacial sediments. If this is not correct, the water depth estimate will be too deep by roughly 1/4 to 1/2 of the sediment thickness, and the depth to the base of the bedrock trough will be too shallow by roughly

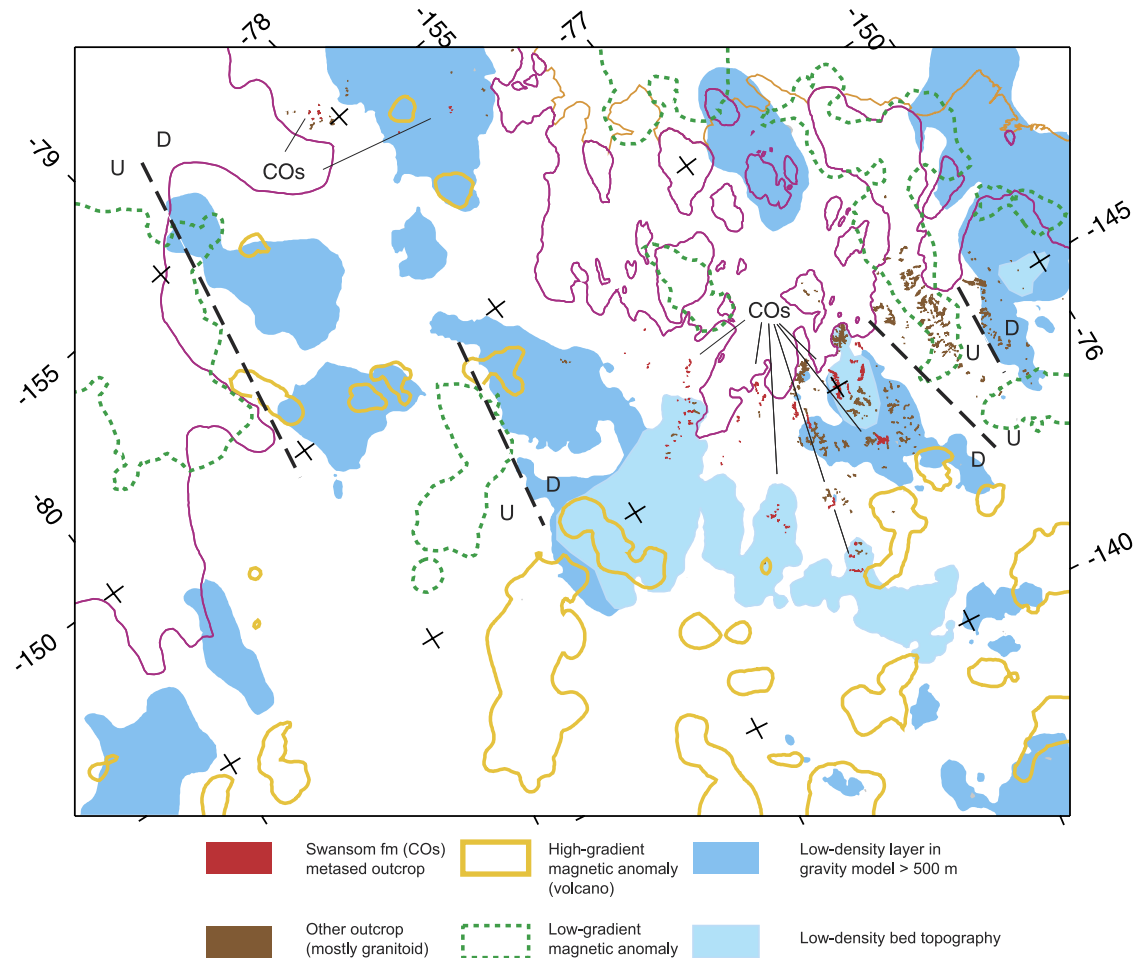


Figure 6. Interpretive map of geophysical features in the survey area (Figures 1b and 2a). Solid yellow outlines are the positive 50-nT magnetic anomaly contours (Figure 2c) outlining high-gradient anomalies that we interpret to indicate volcanic rock beneath the ice. Dashed dark green lines are 50-nT contours outlining lower-gradient positive magnetic anomalies (Figure 2c) that we speculate originate from crustal magnetization contrasts (see text). Blue shaded areas show where a thickness of greater than 500 m of low-density bodies (2300 kg m^{-3}) has been determined from gravity modeling (Figure 5). Light blue areas are sub-sectors of the low-density bodies where gravity and bedrock topography are correlated, constraining low densities to the upper crust (see text). Dark solid areas are outcrops; Swanson Formation outcrops are in red and labeled COs (Cambrian-Ordovician Swanson). Dashed straight lines are inferred faults between crust with low-density bodies and crust with sources of low-gradient magnetic anomalies.

1/2 to 3/4 of the sediment thickness. Though the inferred water depth is moderately uncertain, the positions of the troughs (Figure 3) formerly controlling glacial flow into Sulzberger Bay are known with high confidence. The great depth of the deeper trough to the northwest, downstream from the Hammond Glacier (Figure 2a), supports interpretations of nearly 1 km of ice removal from the western Ford Ranges [e.g., Stone *et al.*, 2003]. Ice thickness near the present value would not

be enough to keep ice grounded at the base of the trough.

[16] Our basement model can be merged with the BEDMAP project model (Figure 4a) [Lythe *et al.*, 2001] (<http://www.antarctica.ac.uk/bedmap/>). That bedrock elevation model lacks the spatial resolution for wMBL that we show here in the coastal regions. The model shows that the bedrock east of our survey in the interior of wMBL is mostly at

elevations above 500 m (Figure 4a). In southern interior wMBL bedrock elevation drops to below sea level approaching the Ross Embayment. The elevation decrease occurs across a zone merely 100 km wide between 77°S to 78°S. The linear trend of the zone is sub parallel to the Transantarctic Mountains, more than 1000 km away to the south and west across the Ross Embayment (Figures 1a and 4a).

2.3.1. Density Variations in the Bedrock

[17] Because the bedrock topography has more than 1 km of local relief in many places (Figure 3), it is possible in these areas to determine average bedrock density from the amplitude of the gravity anomaly. In several areas gravity is well predicted by a standard continental-crust basement density of 2650–2700 kg m⁻³ but other areas are fit best by lower densities of 2300–2400 kg m⁻³ (Figures 5 and 6). We have attempted to quantify the required bedrock density variation by modeling a uniform-density bedrock layer with its thickness varying to approximately fit the shorter-wavelength components of the observed gravity (Figure 5). We chose a density of 2300 kg m⁻³ to fit the anomaly amplitude in portions of a few profiles such as at 320–450 km along profile c (Figure 5c). Assumptions of uniform density for the bedrock layer bounded below by a generally smooth interface with underlying basement reflect convenience in constructing the model rather than our belief that the details are accurate. A higher bedrock density of about 2500 kg m⁻³ could produce similar anomalies if the bedrock-basement interface mirrors the bedrock topography (i.e., it is locally deeper under peaks), which would be plausible if faulting generated the topography. In many areas with limited bed relief or limited coherence between the bed topography and the Free-Air gravity anomaly, only the product of the thickness and the density contrast is constrained.

[18] The density solution for the bedrock layer raises many questions, as there are not extensive outcrops of any rocks with density below 2600 kg m⁻³. The modeled areas of low-density bedrock (Figure 6) are not correlated with outcrops of either Swanson Formation sediments (red in Figure 6) or

the crystalline rocks (brown in Figure 6). Physical interpretation of the modeled low bedrock densities fall in two broad categories: the density model is roughly accurate but the low-density material is unknown and does not crop out; or the mass anomalies are caused instead by topography on a density interface between a uniform low-density upper crust and a denser basement below.

[19] Low-density units may not be found in outcrop if they are much more susceptible to glacial erosion than high-density units. Possible low-density candidates include the epizonal or porphyritic subvolcanic phases of Byrd Coast Granite, Cretaceous sediments resembling those identified by *Pankhurst et al.* [1998] in coastal outcrops ~125 km to the northeast, felsic volcanics or volcanoclastic rocks of Neogene or Cretaceous age found as clasts in moraines of the Fosdick Mountains [*Cowdery and Stone*, 2001], low-grade metasedimentary rocks otherwise equivalent to higher-grade Swanson Formation units, or Tertiary sediments. Samples of Swanson Formation metasediments we measured have densities in the range 2600–2700 kg m⁻³, not any lighter than Ford Granodiorite or Byrd Coast Granite. Low-grade Swanson equivalent is perhaps a least plausible candidate because of its lack of appearance in outcrop or moraines. In places like the central part of the gravity profile presented in Figure 5c, where low bedrock densities are inferred to extend to ridge tops well above sea level, Tertiary sediments are not a plausible component of the bedrock due to a lack of a sediment source. However, low-density younger sediments could exist in areas below sea level near the Ross Ice Shelf and at islands within the Sulzberger Ice shelf.

[20] As an alternative to the low-density bedrock model, the Bouguer gravity lows that we model with shallow, low-density bedrock could result from a faulted or sloping interface between lighter, silicic upper crust and heavier, mafic lower crust. We have assumed this interface is horizontal in wMBL as observed in the Ross Sea [*Trey et al.*, 1999], but this may not be the case. In Figure 6 the light blue areas show the subset of the Bouguer gravity where the Free Air anomaly and bedrock topography are correlated. These are areas where

we have a good constraint on the low bedrock density. For the other darker blue areas in Figure 6, this is not the case, and gravity lows could be explained by middle crust topography between upper, lighter and lower, heavier crust. Simple versions of this alternative predict moderate positive low-gradient magnetic anomalies where the mafic crust is shallower, due to uplift along faults for example. In Figure 6, we highlight several potential faults as dashed lines where inferred areas of low density are adjacent to magnetic anomalies with low gradient that are possibly deeply sourced (dashed dark green lines).

[21] Under most reasonable versions of either of these alternatives, the bedrock density model (Figure 6) maps structural control of differential uplift. If the bedrock densities really are low, those areas have not been exhumed from significant depths, and faulting and uplift most easily explain the density contrast with adjacent areas. In that case the low-density areas are fault-bounded (Figure 6). Faulting would not necessarily deflect an interface between lighter, silicic upper and heavier, mafic lower crust if the middle crust is hot and weak [Gans, 1987; Kaufman and Royden, 1994; Brady *et al.*, 2000]. If instead that interface has substantial topography, it would be most readily explained by differential uplift by faulting, after the middle crust had cooled to develop strength. The distribution of low densities (Figure 6) can be interpreted as an east-west linear pattern parallel to the structural grain of the northern Ford Ranges, even in areas where the bed topography has a fabric in a different direction (Figure 3).

2.3.2. Moho Depth Estimates

[22] Though many local lows in the Bouguer gravity field (Figure 4c) correspond to regions of low densities in the shallow crust (Figures 5 and 6), the Bouguer anomaly is dominated by large negative values where the topography is high, showing isostatic compensation of the topography. Assuming that the Moho accommodates all of this compensation we can estimate Moho topography by fitting the long-wavelength components of the gravity anomaly not predicted by the shallow structure model. To calibrate our Moho model,

we assume that crustal structure near the eastern edge of the Ross Ice Shelf is similar to that mapped near 180°W in the Ross Sea by *Trey et al.* [1999] (Figure 1a). Their seismic refraction and gravity results over a thinly sedimented region of the Central High structure show a crustal thickness of 24 km and a Bouguer anomaly of about +10 mgal. We use the lower crust and mantle densities of 2950 and 3330 kg m⁻³ that they infer from velocity-density relations to derive the Moho model shown in Figure 4d. The wMBL region including the Ford Ranges and most of the Edward VII Peninsula is an area of thin crust (about 25 km) while central Marie Byrd Land crustal thicknesses are 30 km or more. A few of the larger areas of inferred shallow low density bedrock cover a large enough area that lack of control on the shallow structure adds an uncertainty of 1 km or so to the depth of Moho. These larger areas are limited enough that this uncertainty does not significantly affect the interpretation of crustal thickness.

[23] Modeling of marine, land, and airborne gravity data taken together imply that the crust thins by 6 to 9 km (~31 km to ~23 km; $\beta = 1.35$) from locations north and east of the northern Ford Ranges, southwestward to the eastern Ross Sea (Figure 4d). A similar degree of crustal stretching ($\beta = 1.3$) is interpreted from airborne gravity in the West Antarctic Rift farther south adjacent to the Transantarctic Mountains [Studinger *et al.*, 2002]. Half of the thinning occurs in the northern Ford Ranges and half between the southwest side of the Edward VII Peninsula and the Ross Sea continental shelf (Figure 4d). Large differences in original crustal depths between the high-grade metamorphic rocks of the Fosdick Mountains and the low-grade rocks of the adjacent ranges without a comparable deflection of Moho topography under these ranges, suggests that ductile flow of the lower and middle crust transferred material from beneath hanging wall blocks (e.g., Phillips Mountains), to beneath footwall blocks (Fosdick Mountains) [e.g., Jackson *et al.*, 1988]. Plutonism and partial melting in the middle crust during extension contributed to ductile behavior [Smith, 1997]. Although the coverage is extremely sparse, low Bouguer gravity measured farther east (Figure 4c) [Behrendt *et al.*,

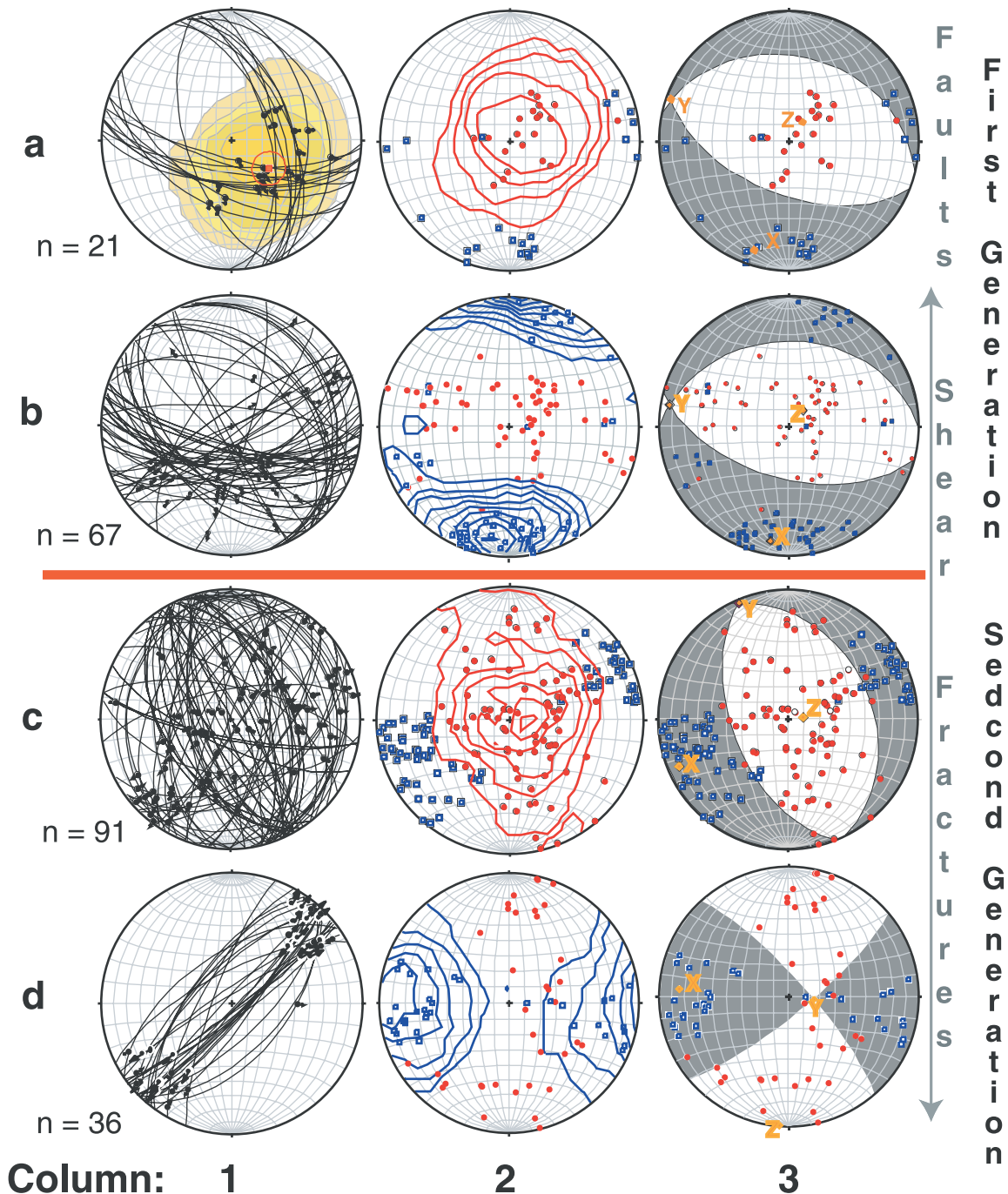
1991a] supports our interpretation of thicker crust toward the interior of wMBL.

3. On Ground Observations

3.1. Brittle Structures of the Ford Ranges

[24] Glacier ice conceals major faults in the region; however, structural studies of brittle faults and

shear fractures in outcrop offer a means to overcome this problem in Antarctica [e.g., *Wilson, 1995*]. Geometrical and kinematic data were collected throughout the Ford Ranges in 1998 and 1999, with the majority of observations collected within isotropic plutonic rocks of the Ford Granodiorite and Byrd Coast Granite. Sub-vertical mafic dikes intruding the granitoids have a regionally



consistent orientation of N12W ($n = 81$ dikes [Siddoway *et al.*, 2003]). Margins of undeformed dikes sometimes exhibit slickensides, a sign that dikes intruded faults. Elsewhere dikes are cut by high angle faults. The mutually crosscutting relationship suggests that the dikes and faults are contemporaneous.

[25] In the Ford Ranges, minor faults are identified as zones of cataclasis or gouge exceeding 15 cm thickness and/or striated planes accommodating >2 m offset. Shear fractures are distinguished as discrete slickenside surfaces restricted to a single plane, generally lacking gouge, with no truncated marker to allow quantification of offset across the striated surface. Few data come from faults and shear surfaces within Swanson Formation, because brittle shear planes typically reactivated preexisting cleavage and slaty partings formed during early Paleozoic orogeny [Bradshaw *et al.*, 1983], making the kinematic significance uncertain. The cleavage in the Swanson Formation is related to an early Paleozoic folding event [Bradshaw *et al.*, 1983; Pankhurst *et al.*, 1998].

3.2. Fault Array, Shear Fracture Arrays, and Kinematic Analysis

[26] Three dominant populations of faults and shear fractures exist in the Ford Ranges based on differing structural attitude and offset sense. These populations are oriented ~ESE-WNW (Figures 7a and 7b); NNW-SSE (Figures 7a and 7c) and NE-SW (Figure 7d), with moderately steep dips. North-northwest and northeast-striking struc-

tures typically cut ESE-oriented structures, so the ESE-WNW population is interpreted to be the oldest set of brittle structures. Kinematic criteria associated with slickensides show down-dip normal slip, strike slip and normal oblique slip [Siddoway, 1999]. Some faults developed two sets of striae. These exhibit well-developed down-dip striae overprinted by delicate strike- to oblique-slip striae.

[27] The first column of Figure 7 summarizes minor fault (row a) and shear fracture (rows b–d) data from the Sarnoff and Denfield Mountains (Figure 2a). Fault data were sufficiently numerous from the Sarnoff Mountains to allow a comparison of faults (row (a) in Figure 7; larger scale features) to shear fractures (row (b) in Figure 7; smaller scale structures with small offset) in order to assess whether the strain record depends on the scale of observation, or is invariant [cf. Marrett and Allmendinger, 1990]. Shear fractures (smaller scale, rows b–d) are widespread throughout the Ford Ranges. Comparing the diagrams in Column 1, row (a) minor faults versus (b) shear fractures, the common element in both data sets is an ESE-striking, S-dipping set of planes with moderately oblique, SE-plunging striae. In addition, there is a second fault set (Figure 7a) striking NNW, dipping NE, that also hosts SE-plunging striae. Striae cluster near the area of intersection of the two fault sets (contoured in yellow in row (a), column 1), and shortening axes cluster (row (a), column 2; see below) indicating that the two form a conjugate array with a compatible direction of shear. Shear

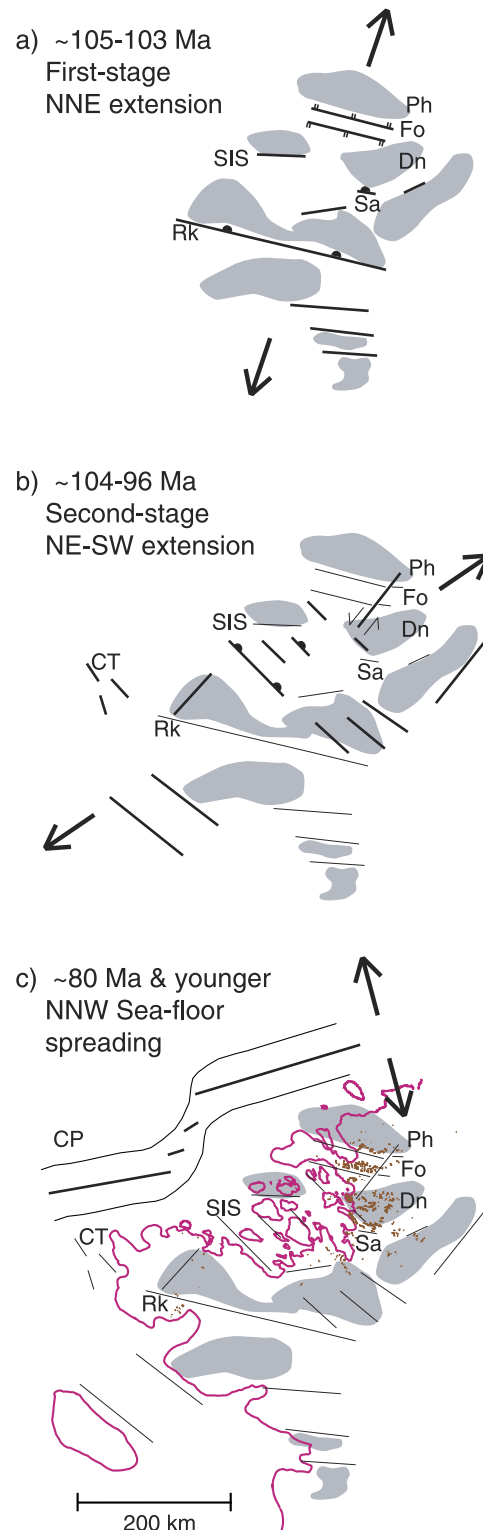
Figure 7. (opposite) Structural and kinematic data, summarized on equal area stereographic projections. The attitudes of brittle faults and shear fractures are summarized in column 1, with attitudes of shear planes shown as great circles; striae, as filled dots; and slip direction, in the direction of the arrow associated with each dot. The contoured yellow area (a, column 1) reflects the density of striae. The square is the mean direction of striae, within 2 sigma (the ellipse around the square). Column 2 shows stretching (blue squares) and shortening (red dots) axes for each fault and shear, contoured on an interval of 2-sigma. Diagrams in Column 3 average the entire fault and shear data to obtain a kinematic solution for the directional maxima, X and Z, for the fields of stretching and shortening, respectively. These are taken as a solution for the principal axes of the regional strain tensor (see text). Data subsets are as follows: (a) early formed E-W to NW-SE minor faults from the Sarnoff Mountains and (b) normal and normal oblique-sense shear fractures from the Sarnoff and Denfield Mountains, that accommodated NNE-SSW stretching. (c) Second generation shear fractures that accommodated normal or normal oblique slip due to NE-SW stretching; Sarnoff and Denfield Mountains. (d) Second generation minor faults and shear fractures that accommodated sinistral strike slip; data from the eastern and central Ford Ranges. Diagrams were prepared using Stereonet v. 6.2, academic version, 1988–2002 by R. W. Allmendinger.

fractures in row (b) exist over a range of orientations, with dominantly down dip or oblique, moderately plunging striae.

[28] Rows (c) and (d) in column 1, Figure 7, provide a summary of shear fracture data from the second generation of brittle structures in the Sarnoff and Denfield ranges. Cross cutting relationships at a small number of sites show that NE- and NNW-striking shear fractures cut those with the ESE attitude shown in Figure 7b; Thus the arrays with NE- and NNW-strike are interpreted as forming during a later, second generation. The fault data in Figure 7 were divided into subsets on the basis of orientation of striae and kinematic sense, as follows: Column 1, row (c), represents shear fractures that have down-dip to oblique striae with normal- to oblique-slip kinematics. Column 1, row (d), portrays shear fractures with strike slip striae, distinguished by their low rake. Importantly, this subset of data came from a group of outcrops along the eastern

margin of the Ford Ranges, nearest to the prominent NE-trending escarpment evident in the bedrock topography (Figure 3). Kinematic criteria consistently showed sinistral-sense offset. The

Figure 8. (opposite) Schematic structural evolution model for the western Marie Byrd Land region, showing relative positions of low-density bodies (shaded) inferred from gravity analysis (Figures 5 and 6) and fault patterns inferred from bedrock trends (Figure 3) and geologic mapping [Luyendyk *et al.*, 1992]. Bold lines indicate faults active at designated times; fine lines are inactive faults. In total, we assume almost 100 kilometers of extension in wMBL leading up to seafloor spreading, consistent with a stretching factor of 1.3 to 1.4. (a) N-S to NNE-SSW extension documented for the Fosdick Mountains (Fo) and Phillips Mountains (Ph) at ~105–103 Ma by Richard *et al.* [1994] and Luyendyk *et al.* [1996], and assumed to have created other E-W boundaries. Abbreviations are as follows: SIS, Sulzberger Ice Shelf; Dn, Denfield Mountains; Rk, Rockefeller Mountains; Sa, Sarnoff Mountains. (b) NE-SW to E-W extension at ~104–96 Ma assumed to have created the NW-SE bed fabric beneath the Sulzberger Ice Shelf (SIS) and areas to the southeast (Figure 2a), faults in the Colbeck Trough (CT) region of the Ross Sea (Figure 1a) [Luyendyk *et al.*, 2001], and minor structures in the southern Ford Ranges [Siddoway, 2000]. Some of the strain may have been partitioned onto NE-trending sinistral faults, compatible with stretching along N65°E. Shorter bold lines show speculative faults of uncertain orientation in regions of thin crust. CT, Colbeck Trough. (c) Seafloor spreading and NNW extension separating the Campbell Plateau (CP) from wMBL, underway before about 79 Ma [Stock and Cande, 2002].



same sense of separation is recorded by an interpreted strike slip fault that interrupts the linear E-W trends of the Phillips and Fosdick Mountains (Figure 8b, below). Apparent offset is >5 km upon the distinctive migmatite gneiss of the Fosdick Range. The generally east-to-west-flowing Balchen Glacier (between Phillips and Fosdick Mountains; Figure 2a) steps left, then returns to east-to-west-flow along the high peaks forming the steep north flank of the Fosdick Mountains.

[29] Graphical and kinematic analyses of the fault and shear slip data are presented in columns two and three of Figure 7 respectively, according to the methods of *Marrett and Allmendinger* [1990] and using the FaultKin 4.1X program of Allmendinger et al. Orientation data for fault and shear planes and striae, together with sense of displacement, are used to calculate the principal axes of shortening (Z, red dots) and extension (X, open squares) (column three Figures 7b, 7c, and 7d) for the incremental strain tensor associated with each fault and shear fracture. The orientation of the strain axes is assumed to be oriented within the plane containing the slickenline and the normal to the fault or shear plane, at 45° to both. The well-defined maxima of extension and/or shortening axes in Figure 7, column two, indicate homogeneity of strain for the arrays.

[30] In column three, the average kinematic solution for each fault and shear population uses linked Bingham statistics to calculate the directional maxima for the field of X and Z strain axes. All faults and shears are weighted equally and assumed to be scale-invariant [*Marrett and Allmendinger*, 1990], an assumption that is validated by the consistent kinematic solutions for both minor faults and shear fractures (larger vs. smaller scale) of the first generation (compare Figure 7a versus 7b, column 3). The first generation faults (Figure 7a) and shear fractures (Figure 7b) record extension along ~N15E, changing to regional extension oriented ~N65E (Figure 7c) during the time of activity of the second-generation structures. During the second event, part of the strain was partitioned on to steep sinistral strike slip faults oriented

~N38E (Figure 7d), compatible with stretching along N65E.

4. Discussion

4.1. Comparison of Structures With Aerogeophysical Lineaments Interpreted as Faults

[31] On the basis of parallelism of predominant trends, we correlate the east-west-oriented mapped faults [*Luyendyk et al.*, 1992], linear gravity anomalies, and bedrock lineaments or escarpments (Figures 3 and 4a) with the first generation structures resulting from NNE extension and represented by the fault array in the Sarnoff Mountains (Figure 7a) and the shear fracture array of the Sarnoff and Denfield Mountains (Figure 7b). The bedrock in these ranges is Devonian Ford granodiorite [*Weaver et al.*, 1991], so there is a possibility that pre-existing major faults (concealed) influence the geometry of the minor structures. The shorter, less throughgoing, NNW-SSE bedrock fabric, known in Sulzberger Bay and continuing onshore to the southeast (Figure 3), we associate with the second generation shear fractures (Figures 7c and 7d) that accommodated normal and normal oblique fault movements during NE-SW crustal stretching. The inferred stretching direction is generally parallel with that determined from mafic dike orientations in the Ford Ranges (excluding Fosdick migmatite dome [*Siddoway*, 2003]). The mutually cross cutting relationships of faults and dikes provides a potential age constraint on timing of NE extension of 104–96 Ma, the prevalent range of ⁴⁰Ar/³⁹Ar ages for the dikes [*Siddoway*, 2003].

[32] During the second extension phase, a component of strain was partitioned onto NE-SW-striking, sinistral, strike-slip faults (Figure 7d). In addition to the NE-trending fault transecting the Phillips and Fosdick Mountains, two NE-trending bedrock lineaments near 140°W (Figure 3) correspond with moderate gradients in the Bouguer gravity anomaly (Figure 4c). Parallelism of these steep bedrock features with the Phillips-Fosdick fault and to a distinctive shear fracture array suggests that some of the bedrock and gravity lineaments may correspond with NE-SW, sinistral,

strike-slip faults. Our interpretation is that the features could represent transfer faults along the eastern Ross Sea rift margin that separate domains of predominant NE-SW stretching accommodated on ~NW-trending normal faults.

[33] The detailed aeromagnetic survey of *Ferraccioli et al.* [2002] (location in Figures 1 and 2) identified lineaments oriented along predominant ~E-W, NNW, and NE trends on Edward VII Peninsula. They inferred the ~E-W- and NNW-oriented features to be normal faults that accommodated ~N-S to NE-SW extension [*Ferraccioli et al.*, 2002] consistent with our regional interpretations shown in Figures 8a and 8b. *Ferraccioli et al.* [2002] interpret the NE-trends to be either normal faults that developed in response to NW-SE stretching or strike-slip (transfer) faults. NW to NNW stretching could have occurred during breakup of New Zealand/Campbell Plateau and Marie Byrd Land (Figure 8c); however if so, that event is not recorded in the nearby Ford Ranges where rock outcrops are more abundant than on Edward VII Peninsula. Similarly, marine surveys adjacent and southwest of Edward VII Peninsula did not identify structures that could have resulted from NW-SE extension [*Luyendyk et al.*, 2001]. We favor an interpretation of the pronounced NE-trending magnetic lineaments as strike slip faults and hypothesize that their movement was sinistral as we observe from our outcrop data.

4.2. Structural Trends and Distribution of Low Density Regions

[34] The approximately east-west alignment of the areas of inferred low-density rock (Figure 6) is parallel to structure and topography in the northern Ford Ranges [*Richard et al.*, 1994] but oblique to bed topography elsewhere. Thermochronology and paleomagnetic data [*Luyendyk et al.*, 1996] from these ranges indicate that the first stage of roughly NNE extension (Figure 8a) occurred 105–103 Ma. Best documented in the northern Ford Ranges, this event could have formed or reactivated ~E-W-striking crustal scale faults, and potentially controlled the preservation of low-density sedimentary rock if extension was fairly similar in style

across the entire study area. Areas where low-density rock is not preserved could reflect simple exhumation of footwall blocks if deformation was dominated by large slip on low angle faults [cf. *Fitzgerald and Baldwin*, 1997], or uplift and erosion of footwall blocks if extension occurred on high-angle faults (Figure 6). The lack of penetrative solid-state fabrics in the exposed crystalline rocks of wMBL favors an interpretation of high-angle faulting, but the possibility exists that shear zones containing those fabrics are concealed by ice or have been removed by erosion. Clastic sediments derived from uplifted crystalline bedrock have not been observed directly but they could make up a portion of the low-density material required by the gravity models. The generally east-west distribution of modeled low-density regions is oblique to NW-SE trends of the bed topography southeast of the Sulzberger Ice Shelf and the NW-SE to N-S trends of the mostly sediment-filled basement topography in the Colbeck Trough region mapped by *Luyendyk et al.* [2001]. The contrasting trends indicate a multistage history of extension in the eastern Ross Sea rift.

4.3. Tectonics of the Eastern Regions of the Ross Sea Rift

[35] The findings from aerogeophysical surveys and structural geology studies in the Ford Ranges suggest that the crustal architecture along the eastern margin of the Ross Sea rift developed through NNE-SSW and NE-SW regional extension, affecting Cretaceous and older rock units. Crustal-scale structures in the northern Ford Ranges were produced during the earlier NNE-SSW stretching. The extension phase oriented N65°E–S65°W (NE extension) corresponds to mafic dikes and second-generation brittle structures on land in the Ford Ranges, and ~N-S trending, fault-bounded basins and ridges in the eastern Ross Sea basement. The latter are identified by marine geophysical surveys in the region of the Colbeck Trough near Edward VII Peninsula where the faulted basement is unconformably overlain by a few hundred meters of undeformed Late Tertiary glacial marine and glacial sediments [*Luyendyk et al.*, 2001]. *Luyendyk et al.* [2001] interpreted the

faulted basement pattern offshore to be a product of roughly east-west extension in early Late Cretaceous time.

[36] We correlate the offshore and onshore faults, and infer that the $^{40}\text{Ar}/^{39}\text{Ar}$ age of the Ford Ranges mafic dikes, in mutual crosscutting relationship with faults on land, constrains the time of NE extension to 104–96 Ma. The faults and dikes trend at a high angle to the rifted continental margin in wMBL, and the extension direction they record is nearly orthogonal to the orientation of seafloor spreading that initiated along the margin at ~ 79 Ma [Stock and Cande, 2002]. We attribute the first and second-generation structures to intracontinental extension that led to the formation of the Ross Sea rift in the eastern Ross Sea (Figures 8a and 8b).

[37] The areal extent of tectonism in the eastern Ross Sea and wMBL region during this time interval is evident from thermochronologic data. Mylonitic gneisses derived from Byrd Coast Granite, dredged from the inner rocky wall of the Colbeck Trough (Figure 1a) [Siddoway et al., 2003; Luyendyk et al., 2001] have $^{40}\text{Ar}/^{39}\text{Ar}$ K-feldspar and biotite ages of 98–95 Ma [Siddoway et al., 2003], like the Fosdick Mountains migmatites [Richard et al., 1994]. Further west at Deep Sea Drilling Project site 270 in the Eastern Basin, basement-derived tectonites with similar early Late Cretaceous cooling ages show a brittle upon ductile textural overprint, interpreted as evidence of exhumation in a detachment system [Fitzgerald and Baldwin, 1997]. On Edward VII Peninsula inland from the Colbeck trough, a contrasting apatite fission track-cooling pattern between northern and central outcrops is attributed to mid-Cretaceous fault displacements [Adams et al., 1995; Lisker and Olesch, 1998].

[38] In western Marie Byrd Land, the episode of continental extension responsible for denudation and rapid cooling across the region apparently was distinct from the subsequent breakup with the Campbell Plateau/New Zealand. Because rift-related structures in the eastern Ross Sea trend at a high angle to and are abruptly truncated at the passive margin edge [Luyendyk et al., 2001],

we conclude that faults, ridges, and valleys recording NE-SW to E-W extension (Figure 8b) predate the passive margin edge, which according to [Stock and Cande, 2002] formed at or just before the start of seafloor spreading at 79 Ma (Figure 8c). Since onset of spreading, little/no deformation has occurred in the eastern Ross Sea [Lawver and Gahagan, 1994; Luyendyk et al., 2001], other than minor Neogene-modern fault activity [Siddoway, 2000] and seismicity [Anandakrishnan and Winberry, 2002] that occurs within the contemporary West Antarctic rift system. There are presently no data from MBL that indicate activity in Eocene time, a time of uplift and exhumation in the Transantarctic Mountains [Fitzgerald, 1992]. The clear contrast in cooling history of MBL to the Transantarctic Mountains, on the eastern versus western margins of the Ross Sea rift, suggests that the observed asymmetry of the Ross Sea rift developed in multiple events with differing ages.

[39] The record of NNE- to NE- extension in the Ford Ranges of western MBL differs from that in the Ruppert Coast to the east (Figure 1a), where N-S extension is inferred from the predominant \sim E-W, margin-parallel orientation of mafic dikes [Storey et al., 1999]. Of 108–104 Ma age, the dikes are interpreted to record onset of breakup between MBL and New Zealand [Storey et al., 1999]. The contrasting orientations of approximately same-aged dikes in coastal MBL, we attribute to the differing tectonic character and setting of the two regions. Pankhurst et al. [1998], distinguish two distinct tectonic provinces within MBL, noting that the western Ross province including the Ford Ranges is of continental affinity, while the eastern Amundsen province including the Ruppert Coast and eastern MBL has the character of a marginal arc and close ties to New Zealand basement geology. If a major tectonic boundary separated the two provinces, it is possible that differing tectonic stress environments existed in each province during mafic dike emplacement. Possible external influences affecting the crust in the western MBL and the Ross Sea include onset of extension between the Australian and Antarctic plates [Stock and Cande, 2002] and cessation

of subduction of the Phoenix plate under the Gondwana margin [Bradshaw, 1989; Luyendyk, 1995].

5. Conclusions

[40] We propose that coastal wMBL including the Ford Ranges and Edward VII Peninsula provides regional exposures of the basement geology and structure of the eastern Ross Sea rift. The combined observations of bedrock topography, gravity anomaly, and geological contrasts in the northern Ford Ranges suggest that coastal wMBL is a region of extended crust and that the boundary of pronounced crustal extension is located just beyond the northern Ford Ranges 300 to 350 km northeast of the grounding line in the eastern Ross Sea. A sub-ice volcanic field identified from the magnetic anomalies is situated along or near that boundary. Sparse gravity and bedrock elevations from interior (east) wMBL suggest further that the boundary of extended crust trends ESE inland from the coast. Using a bedrock elevation of 500 m (Figure 4a) as the mark of the extended crust boundary we can measure the width of the Ross Sea rift to be approximately 1200 kilometers to the Transantarctic Mountains (Figure 1a). The extension history in our study region differs from that to the east in the Ruppert Coast of MBL, which is dominated by a record of crustal stretching related to breakup with New Zealand.

[41] Differing tectonic histories also are the likely explanation of the pronounced asymmetry in the topography at the opposite boundaries of the Ross Sea rift. The middle Cretaceous extension episode is well represented in the basement geology of wMBL where features of the Ross Sea rift are exposed. The Transantarctic Mountains and structures such as the Terror Rift in the Victoria Land Basin, are younger Tertiary features [Barrett *et al.*, 2000; Hamilton *et al.*, 2001; Fitzgerald, 1992, 2002] that overprint or reactivate the Mesozoic features. Eocene-Oligocene spreading in the Adare Trough north of the western Ross Sea continental margin [Cande *et al.*, 2000] strongly influenced the subsidence of the Victoria Land Basin [Hamilton *et al.*, 2001], whereas this had little effect in the

eastern Ross Sea and wMBL [Luyendyk *et al.*, 2001].

Acknowledgments

[42] We gratefully acknowledge the Support Office for Aero-geophysical Research (SOAR) at the University of Texas, Austin and Dr. Don Blankenship for his management of SOAR field acquisition and preliminary processing work. We also thank pilots Scott Lippa, Duncan Russell, Henry Perk and Max Wenden (Ken Borek Air) who flew the aerogeophysics and supported the ground party; Dave Morse and Scott Kempf of SOAR and Bob Arko of Columbia University for preliminary data processing; and Marcy Davis of UC Santa Barbara and University of Texas, who assisted in the field program. From the U.S. Antarctic Program, Steve Niles, Sarah Harvey, and Sue Root deserve special mention along other McMurdo support personnel. Anne Whitehead and Louis Sass III (Colorado College) contributed to the structural geology program, together with Mike Roberts, our mountain guide. Dr. John Behrendt provided us with MBL land traverse data. Sincere thanks go to Dr. Dick van der Wateren for many stimulating discussions and his enthusiastic participation during the first ground field season. We also wish to thank Drs. Robin Bell, Fred Davey, Carol Finn, and Michael Studinger for helpful comments. Research supported by National Science Foundation Office of Polar Program grants NSF OPP 9615281 to Luyendyk and NSF OPP 9615282 to Siddoway. Contribution 518 of the Institute for Crustal Studies.

References

- Adams, C. J., D. Seward, and S. D. Weaver, Geochronology of Cretaceous granites and metasedimentary basement on Edward VII Peninsula, Marie Byrd Land, West Antarctica, *Antarct. Sci.*, 7, 265–277, 1995.
- Anandakrishnan, S., and P. Winberry, Results of a seismic deployment in West Antarctica: Ice sheet effects on high resolution imaging, *Eos Trans. AGU Spring Meet. Suppl.*, 82(47), Abstract U42A-11, 2002.
- Barrett, P. J., M. Massimo Sarti, and S. Wise, Studies from the Cape Roberts Project, Ross Sea, Antarctica: Initial report on CRP-3, in *Terra Antarctica*, pp. 209, Terra Antarctica, Siena, Italy, 2000.
- Behrendt, J. C., W. E. LeMasurier, A. K. Cooper, F. Tessensohn, A. Trehu, and D. Damaske, Geophysical studies of the West Antarctic Rift System, *Tectonics*, 10, 1257–1273, 1991a.
- Behrendt, J. C., W. E. LeMasurier, A. K. Cooper, F. Tessensohn, A. Trehu, and D. Damaske, The West Antarctic Rift System: A review of geophysical investigations, in *Contributions to Antarctic Research II*, *Antarct. Res. Ser.*, vol. 53, edited by D. H. Elliot, pp. 67–112, AGU, Washington, D. C., 1991b.
- Beitzel, J. E., Geophysical investigations in Marie Byrd Land, Antarctica, Ph.D. dissertation thesis, Univ. of Wisconsin, Madison, 1972.
- Bell, R. E., V. A. Childers, R. A. Arko, D. D. Blankenship, and J. M. Brozena, Airborne Gravity and Precise Positioning for

- Geological Applications, *J. Geophys. Res.*, *104*(B7), 15,281–15,292, 1999.
- Bentley, C. R., Crustal structure of Antarctica, *Tectonophysics*, *20*, 229–240, 1973.
- Bentley, C. R., Configuration and structure of the subglacial crust, in *The Geology of Antarctica*, edited by R. J. Tingey, pp. 335–364, Clarendon, Oxford, England, 1991.
- Bradshaw, J. D., Cretaceous geotectonic patterns in the New Zealand region, *Tectonics*, *8*, 803–820, 1989.
- Bradshaw, J. D., P. B. Andrews, and B. D. Field, Swanson Formation and related rocks of Marie Byrd Land and a comparison with the Robertson Bay Group of Northern Victoria Land, in *Antarctica Earth Science*, edited by R. L. Oliver et al., pp. 274–279, Aust. Acad. of Sci., Canberra, 1983.
- Brady, R. J., B. P. Wernicke, M. McNutt, J. Mutter, and G. Correa, Crustal structure of the Basin and Range to Colorado Plateau transition in the Lake Mead region from BARGE seismic reflection data, *Geochem. Geophys. Geosyst.*, *1*, Paper number 2000GC000078, 2000.
- Cande, S. C., J. M. Stock, D. Müller, and T. Ishihara, Cenozoic Motion between East and West Antarctica, *Nature*, *404*, 145–150, 2000.
- Childers, V. A., R. E. Bell, and J. M. Brozena, Airborne gravimetry: An investigation of filtering, *Geophysics*, *64*, 61–69, 1999.
- Cowdery, S. G., and J. O. Stone, Geological insight into the Holocene glacial history of West Antarctica based on moraine studies, petrography of erratics, and cosmogenic dating, *Geol. Soc. Am. Abstr. Programs*, *33*(5), A-13, 2001.
- Dalziel, I. W. D., and L. Lawver, The Lithospheric Setting of the West Antarctic Icesheet, in *The West Antarctic Ice Sheet: Behavior and Environment*, *Antarct. Res. Ser.*, vol. 77, edited by R. B. Alley and R. A. Bindshadler, pp. 29–44, AGU, Washington, D. C., 2001.
- Davey, F. J., and G. Brancolini, The Late Mesozoic and Cenozoic structural setting of the Ross Sea region, in *Geology and Seismic Stratigraphy of the Antarctic Margin*, *Antarct. Res. Ser.*, vol. 68, edited by A. K. Cooper, P. F. Barker, and G. Brancolini, pp. 167–182, AGU, Washington, D. C., 1995.
- Ferraccioli, F., E. Bozzo, and D. Damaske, Aeromagnetic signatures over western Marie Byrd Land provide insight into magmatic arc basement, mafic magmatism, and structure of Eastern Ross Sea Rift flank, *Tectonophysics*, *347*, 139–165, 2002.
- Fitzgerald, P. G., The Transantarctic Mountains of Southern Victoria Land: The application of apatite fission track analysis to a rift shoulder uplift, *Tectonics*, *11*, 634–662, 1992.
- Fitzgerald, P. G., Tectonics and landscape evolution of the Antarctic Plate since the breakup of Gondwana with an emphasis on the West Antarctic Rift System and the Transantarctic Mountains, in *Antarctica at the Close of a Millennium: Proceedings of the 8th International Symposium on Antarctic Earth Sciences*, Wellington, 1999, edited by J. A. Gamble, D. N. B. Skinner, and S. Henrys, pp. 453–469, Royal Soc. of New Zealand, Wellington, 2002.
- Fitzgerald, P. G., and S. L. Baldwin, Detachment Fault Model for the Evolution of the Ross Embayment, in *The Antarctic Region: Geological Evolution and Processes*, edited by C. A. Ricci, pp. 555–564, Terra Antarct., Siena, Italy, 1997.
- Gans, P. B., An open system, two-layer crustal stretching model for the eastern Great Basin, *Tectonics*, *6*, 1–12, 1987.
- Greischar, L. L., C. R. Bentley, and L. R. Whiting, An analysis of gravity measurements on the Ross Ice Shelf, Antarctica, in *Contributions to Antarctic Research III*, *Antarct. Res. Ser.*, vol. 57, edited by D. H. Elliot, pp. 105–155, Am. Geophys. Union, Washington, D. C., 1992.
- Hamilton, R. J., B. P. Luyendyk, C. C. Sorlien, and L. R. Bartek, Cenozoic Tectonics of the Cape Roberts Rift Basin, and Transantarctic Mountains Front, Southwestern Ross Sea, Antarctica, *Tectonics*, *20*, 325–342, 2001.
- Jackson, J. A., N. J. White, Z. Garfunkel, and H. Anderson, Relations Between Normal Fault Geometry, Tilting and Vertical Motions in Extensional Terrains: An Example from the Southern Gulf of Suez, *J. Struct. Geol.*, *10*, 155–170, 1988.
- Kaufman, P. S., and L. H. Royden, Lower Crustal Flow in an Extensional Setting: Constraints from the Halloran Hills Region, Eastern Mojave Desert, California, *J. Geophys. Res.*, *66*, 15,723–15,739, 1994.
- Lawver, L. A., and L. M. Gahagan, Constraints on timing of extension in the Ross Sea region, *Terra Antarct.*, *1*, 545–552, 1994.
- LeMasurier, W. E., and D. C. Rex, Evolution of linear volcanic ranges in Marie Byrd Land, West Antarctica, *J. Geophys. Res.*, *94*, 7223–7236, 1989.
- LeMasurier, W. E., and D. C. Rex, Late Cenozoic volcanism on the Antarctic Plate: An overview, in *Volcanoes of the Antarctic Plate and Southern Oceans*, *Antarct. Res. Ser.*, vol. 48, edited by W. E. LeMasurier and J. W. Thompson, pp. 1–17, Am. Geophys. Union, Washington, D. C., 1990.
- Lemoine, F. G., et al., The development of the joint NASA GSFC and the National Imagery and Mapping Agency (NIMA) geopotential model EGM96, NASA, Greenbelt, Md., 1998.
- Lisker, F., and M. Olesch, Cooling and denudation history of Edward VII Peninsula, Marie Byrd Land, based on apatite fission tracks, in *Advances in Fission-Track Geochronology*, edited by P. Van den haute and F. De Corte, pp. 225–240, Kluwer Acad., Norwell, Mass., 1998.
- Liu, H., K. C. Jezek, and B. Li, Development of an Antarctic digital elevation model by integrating cartographic and remotely sensed data: A geographic information system based approach, *J. Geophys. Res.*, *104*, 23,199–23,213, 1999.
- Luyendyk, B. P., Hypothesis for Cretaceous rifting of east Gondwana caused by subducted slab capture, *Geology*, *23*, 373–376, 1995.
- Luyendyk, B. P., S. M. Richard, C. H. Smith, and D. L. Kimbrough, Geological and geophysical investigations in the northern Ford Ranges, Marie Byrd Land, West Antarctica, in *Recent Progress in Antarctic Earth Science: Proceedings of the 6th Symposium on Antarctic Earth Science*, Saitama, Japan, 1991, edited by Y. Yoshida,

- K. Kaminuma, and K. Shiraishi, pp. 279–288, Terra Sci., Tokyo, Japan, 1992.
- Luyendyk, B. P., S. Cisowski, C. H. Smith, S. M. Richard, and D. L. Kimbrough, Paleomagnetic study of the northern Ford Ranges, western Marie Byrd Land, West Antarctica: A middle Cretaceous pole, and motion between West and East Antarctica?, *Tectonics*, *15*, 122–141, 1996.
- Luyendyk, B. P., C. C. Sorlien, D. S. Wilson, L. R. Bartek, and C. H. Siddoway, Structural and tectonic evolution of the Ross Sea rift in the Cape Colbeck region, Eastern Ross Sea, Antarctica, *Tectonics*, *20*, 933–958, 2001.
- Luyendyk, B. P., D. S. Wilson, and R. Decesari, New Maps of Gravity and Bedrock-Bathymetry of the Ross Sea Sector of Antarctica, *Eos Trans. AGU, Fall Meet. Suppl.*, *83*(47), F1357, 2002.
- Luyendyk, B. P., C. H. Smith, and G. Druivenga, Gravity measurements on King Edward VII Peninsula, Marie Byrd Land, West Antarctica, during GANOVEX VII, *Geol. Jahrb.*, *B95*, 101–126, 2003.
- Lythe, M. B., et al., BEDMAP: A new ice thickness and subglacial topographic model of Antarctica, *J. Geophys. Res.*, *106*, 11,335–11,351, 2001.
- Marrett, R. A., and R. W. Allmendinger, Kinematic analysis of fault-slip data, *J. Struct. Geol.*, *12*, 973–986, 1990.
- Pankhurst, R. J., S. D. Weaver, J. D. Bradshaw, B. C. Storey, and T. R. Ireland, Geochronology and geochemistry of pre-Jurassic superterranes in Marie Byrd Land, Antarctica, *J. Geophys. Res.*, *103*, 2529–2547, 1998.
- Panter, K. S., S. R. Hart, P. R. Kyle, J. Blusztajn, and T. I. Wilch, Geochemistry of late Cenozoic basalts from the Crary Mountains: Characterization of mantle sources in eastern Marie Byrd Land, Antarctica, *Chem. Geol.*, *165*, 215–241, 2000.
- Parker, R. L., The rapid calculation of potential anomalies, *Geophys. J. R. Astron. Soc.*, *31*, 447–455, 1973.
- Richard, S. M., C. H. Smith, D. L. Kimbrough, P. G. Fitzgerald, B. P. Luyendyk, and M. O. McWilliams, Cooling history of the northern Ford Ranges, Marie Byrd Land, West Antarctica, *Tectonics*, *13*, 837–857, 1994.
- Siddoway, C. H., Structural evolution of the Ford Ranges, Marie Byrd Land, from brittle kinematic analysis, paper presented at 9th International Symposium on Antarctic Earth Sciences, Sci. Comm. on Antarctic Res., Potsdam, Germany, 2003.
- Siddoway, C. S., Late Cretaceous-Cenozoic Structural Evolution of western Marie Byrd Land (abstract), in *8th International Symposium on Antarctic Earth Sciences*, edited by D. N. B. Skinner, pp. 281, Victoria Univ., Wellington, New Zealand, 1999.
- Siddoway, C. S., Tectonic evolution of Marie Byrd Land, West Antarctica: Disassembly of the Mesozoic margin and Cenozoic activity related to the West Antarctic Rift System [extended abstract on CD-ROM], paper presented at 31st International Geological Congress, Int. Union of Geol. Sci., Rio de Janeiro, August 7–16, 2000.
- Siddoway, C. S., S. L. Baldwin, P. G. Fitzgerald, C. M. Fanning, and B. P. Luyendyk, Ross Sea mylonites and the timing of continental extension between East and West Antarctica, *Geology*, in press, 2003.
- Smith, C. H., Migmatites at the amphibole-granulite transition, Fosdick Metamorphic Complex, West Antarctica, in *Recent Progress in Antarctic Earth Science: Proceedings of the 6th Symposium on Antarctic Earth Science, Saitama, Japan, 1991*, edited by Y. Yoshida, K. Kaminuma, and K. Shiraishi, pp. 295–301, Terra Sci., Tokyo, Japan, 1992.
- Smith, C. H., Mid-Crustal Processes During Cretaceous Rifting, Fosdick Mountains, Marie Byrd Land, in *The Antarctic Region Geological Evolution and Processes*, edited by C. A. Ricci, pp. 313–320, Terra Antart., Siena, Italy, 1997.
- Stock, J. M., and S. C. Cande, Tectonic History of Antarctic Seafloor in the Australia-New Zealand-South Pacific Sector: Implications for Antarctic Continental Tectonics, in *Antarctica at the Close of a Millennium: Proceedings of the 8th International Symposium on Antarctic Earth Sciences, Wellington, 1999*, edited by J. A. Gamble, D. N. B. Skinner, and S. Henrys, pp. 251–259, R. Soc. of New Zealand, Wellington, 2002.
- Stone, J. O., G. A. Balco, D. E. Sugden, M. W. Caffee, L. C. Sass III, S. G. Cowdery, and C. Siddoway, Holocene deglaciation of Marie Byrd Land, West Antarctica, *Science*, *299*, 99–102, 2003.
- Storey, B. C., P. T. Leat, S. D. Weaver, R. J. Pankhurst, J. D. Bradshaw, and S. Kelley, Mantle Plumes and Antarctica-New Zealand rifting: Evidence from mid-Cretaceous mafic dykes, *J. Geol. Soc. London*, *156*, 659–671, 1999.
- Studinger, M., R. E. Bell, C. A. Finn, and D. D. Blankenship, Mesozoic and Cenozoic extensional tectonics of the West Antarctic rift system from high-resolution airborne geophysical mapping, in *Antarctica at the Close of a Millennium: Proceedings of the 8th International Symposium on Antarctic Earth Sciences, Wellington, 1999*, edited by J. Gamble, D. N. B. Skinner, and S. A. Henrys, pp. 563–569, The R. Soc. of New Zealand, Wellington, New Zealand, 2002.
- Tessensohn, F., and G. Worner, The Ross Sea rift system, Antarctica: Structure, evolution, and analogs, in *Geological Evolution of Antarctica*, edited by M. R. A. Thompson, J. A. Crame, and J. W. Thompson, pp. 273–278, Cambridge Univ. Press, New York, 1991.
- Trey, H., A. K. Cooper, G. Pellis, B. Della Vedova, G. Cochrane, G. Brancolini, and J. Makris, Transect across the West Antarctic rift system in the Ross Sea, Antarctica, *Tectonophysics*, *301*, 61–74, 1999.
- Wade, F. A., C. A. Cathey, and J. B. Oldham, Reconnaissance geologic map of the Guest Peninsula quadrangle, Marie Byrd Land, Antarctica, Map A-7, U. S. Antarc. Res. Program, Reston, Va., 1977a.
- Wade, F. A., C. A. Cathey, and J. B. Oldham, Reconnaissance geologic map of the Boyd Glacier quadrangle, Marie Byrd Land, Antarctica, Map A-6., U. S. Antarc. Res. Program, Reston, Va., 1977b.
- Wade, F. A., C. A. Cathey, and J. B. Oldham, Reconnaissance geologic map of the Alexandra Mountains quadrangle, Marie Byrd Land, Antarctica, Map A-5, U. S. Antarc. Res. Program, Reston, Va., 1977c.
- Wade, F. A., C. A. Cathey, and J. B. Oldham, Reconnaissance geologic map of the Gutenko Nunataks quadrangle, Marie

- Byrd Land, Antarctica, Map A-11, U. S. Antarc. Res. Program, Reston, Va., 1978.
- Weaver, S. D., J. D. Bradshaw, and C. J. Adams, Granitoids of the Ford Ranges, Marie Byrd Land, Antarctica, in *Geological Evolution of Antarctica*, edited by M. R. A. Thompson et al., pp. 345–351, Cambridge Univ. Press, Cambridge, Mass., 1991.
- Weaver, S. D., B. C. Storey, R. J. Pankhurst, S. B. Mukasa, V. J. DiVenere, and J. D. Bradshaw, Antarctica-New Zealand rifting and Marie Byrd Land lithospheric magmatism linked to ridge subduction and mantle plume activity, *Geology*, **22**, 811–814, 1994.
- Whitehead, A. L., C. S. Siddoway, and F. W. van der Wateren, Kinematic Analysis of Small-Scale Brittle Structures in the Ford Ranges, Marie Byrd Land (abstract), in *8th International Symposium on Antarctic Earth Sciences, July 5–9, 1999*, edited by D. N. B. Skinner, pp. 316, Victoria Univ., Wellington, New Zealand, 1999.
- Wilson, D. S., B. P. Luyendyk, C. S. Siddoway, and M. Davis, Preliminary Results From an Aerogeophysical Survey of Western Marie Byrd Land, Antarctica, *Eos Trans. AGU, Fall Meet. Suppl.*, **81**(48), F405, 2000.
- Wilson, D. S., B. P. Luyendyk, C. C. Sorlien, and J. Stone, Geophysical Observations Supporting Significant Variation in ice Thickness of Western Marie Byrd Land, Antarctica, *Eos Trans. AGU, Fall Meet. Suppl.*, **82**(42), F793, 2001.
- Wilson, D. S., B. P. Luyendyk, and C. C. Sorlien, Formation of Bedrock Plateaus within the Ross Sea Embayment, Antarctica, by Marine Erosion in Late Tertiary Time, paper presented at 9th International Symposium on Antarctic Earth Sciences, Sci. Comm. on Antarctic Res., Potsdam, Germany, 2003.
- Wilson, T., Cenozoic transtension along the Transantarctic Mountains-West Antarctic rift boundary, southern Victoria Land, Antarctica, *Tectonics*, **14**, 531–545, 1995.